High Temperature Seismic Monitoring for Enhanced Geothermal Systems

Implementing a Control Feedback Loop to a Prototype Tool by Sandia National Laboratories

Panit Howard

Thesis submitted to the faculty of the Virginia Polytechnic Institute and State University
in partial fulfillment of the requirements for the degree of

Masters of Science
in
Mechanical Engineering

Dennis Hong

Alfred L. Wicks

Frank Maldonado

High Temperature Seismic Monitoring for Enhanced Geothermal Systems

Implementing a Control Feedback Loop to a Prototype Tool by Sandia National Laboratories

Panit Howard

Abstract

Geothermal energy can make an important contribution to the U.S. energy portfolio. Production areas require seismic monitoring tools to develop and monitor production capability. This paper describes modifications made to a prototypical seismic tool to implement improvements that were identified during previous tool applications. These modifications included changing the motor required for mechanical coupling the tool to a bore-hole wall. Additionally, development of a closed-loop process control utilized feedback from the contact force between the coupling arm and bore-hole wall. Employing a feedback circuit automates the tool deployment/anchoring process and reduces reliance on the operator at the surface. The tool components were tested under high temperatures and an integrated system tool test demonstrated successful tool operations.

Acknowledgements

This thesis would not have been possible without the help and support of the kind people around me.

Above all, I would like to thank my parents and sister who have given me their unwavering support and love throughout my academic and professional career. I want to thank my manager Dr. Christi Leigh, who strongly influenced my decision to further my education and her dedicated support to my academic and professional development. I wish to thank Doug Blankenship and Frank Maldonado for providing a project where I was able to contribute to the advancement of geothermal system monitoring. Additionally, I need to extend a big thanks to the rest of the team in the Geothermal Energy Department at Sandia National Laboratories. They brought me in, treated me like one of their own, and provided the support necessary for me to complete my project on time.

This thesis would not have been possible without the support and patience of my advisors Dr. Dennis Hong and Dr. Alfred L. Wicks, granting me the opportunity to work on a project of my choosing. I'd like to recognize Cathy Hill, the Mechanical Engineering Department chief coordinator and administrative assistant, whom assisted me by obtaining signatures and submitting the required forms enabling my success in meeting the administrative requirements associated with submitting and defending this thesis.

I acknowledge Sandia National Laboratories for their financial support, allowing me to focus on my education and sponsoring this work. Lastly, I want to thank my all my friends who were supportive while I was at school.

Sandia National Laboratories is a multi-program laboratory managed and operated by Sandia Corporation, a wholly owned subsidiary of Lockheed Martin Corporation, for the U.S. Department of Energy's National Nuclear Security Administration under contract DE-AC04-94AL85000.

TABLE OF CONTENTS

LIST OF FIGURES

LIST OF TABLES

Chapter 1. INTRODUCTION

The Department of Energy (DOE) sponsored a study examining the potential of geothermal energy to meet future energy needs of the United States. The study concluded that geothermal energy could potentially provide 100,000 megawatts of electricity within the U.S. Figure 1 shows locations of geothermal potential with yellows and reds representing areas with the most significant potential (Jefferson W. Tester, 2006).

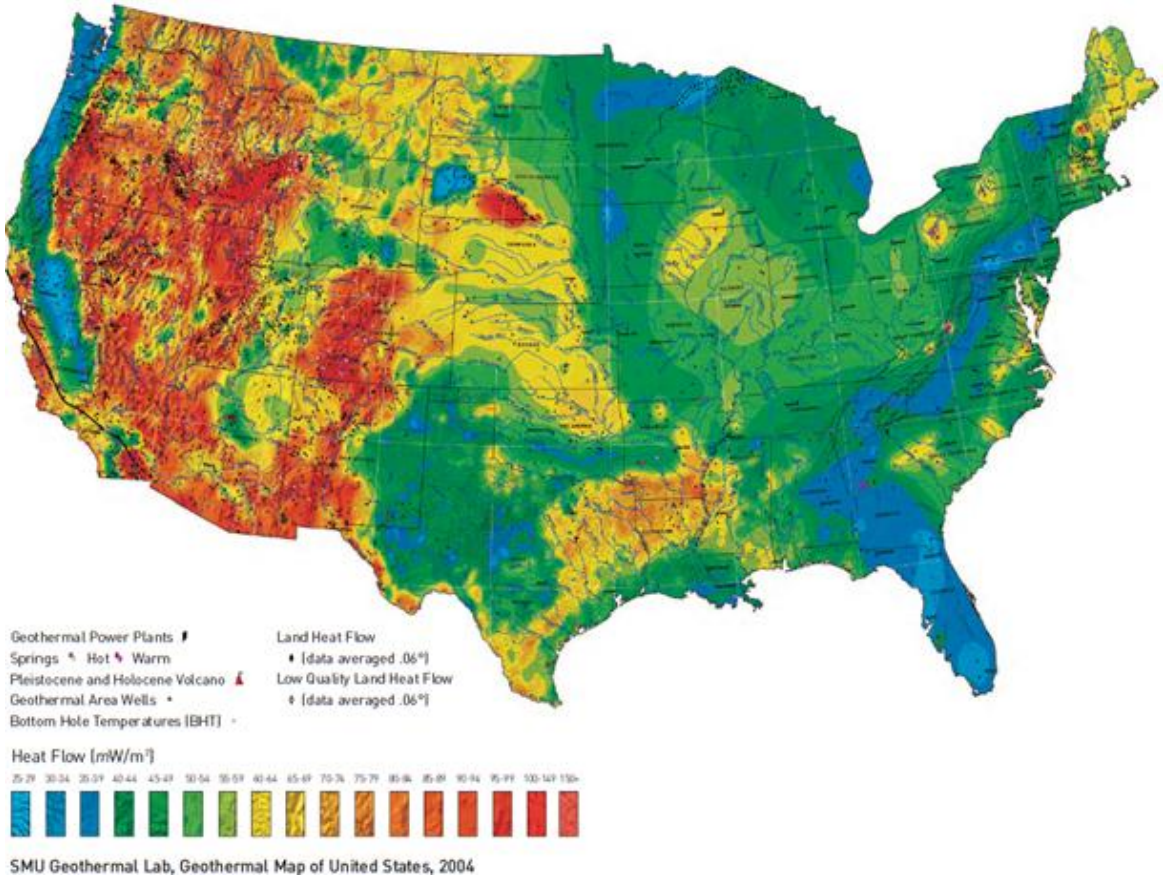

Figure 1: Geothermal Map of United States

The study noted the benefits of geothermal energy: 1) it is renewable – through proper reservoir management, the rate of energy extraction can be balanced with a reservoir's natural heat recharge rate, 2) it is reliable for baseload power – geothermal power plants produce electricity consistently, regardless of weather conditions or time of day, 3) it is produced domestically – geothermal power production doesn't rely on imported fuel and creates high paying jobs, 4) it has a small footprint – geothermal power plants are physically compact; using less land per

gigawatt-hour than conventional energy sources, and 5) it is clean – modern geothermal power plants emit no greenhouse gasses (U.S. Department of Energy, 2012).

1.1 Motivation Behind Research

Building on the initial assessment made by the DOE, scientists with the U.S. Geological Survey (USGS) completed an assessment of geothermal potential based on technical advancements in geothermal technology available in 2008. Conventional methods for extracting geothermal resources depend on hydrothermal fluid circulation that occurs naturally, which limits the viable locations for geothermal energy production. With advances in technology, enhanced geothermal systems (EGS) have become viable through implementation of technology that fractures the hot rock mass and introduces a hydrothermal fluid. Geothermal reservoirs can then be created in regions characterized by high temperature, but low permeability rock formations where circulating fluids do not naturally occur. Enhanced geothermal systems require engineering to develop the permeability necessary for circulation of hot water and the recovery of heat for power. The assessment indicates that electric power generation potential with enhanced geothermal systems to be 517,800 megawatts, more than 5 times the previous estimate or about half of the country's electricity needs (Williams, Reed, Robert, & Jacob, 2008).

Currently there are two primary thrusts of research being pursued to advance enhanced geothermal systems: 1) to determine if impermeable hydrothermal systems can be made productive by means of stimulation through hydraulic fracturing and 2) to further engineer underground conditions by introduction of circulating fluids that result in hydrothermal systems that can be controlled and harnessed by power plants. Monitoring tools capable of withstanding high temperature environments are needed to enable the monitoring of fracture propagation during the stimulation process (Majer, et al., 2006).

1.2 Scope

The development of geothermal field systems requires the tracking of fracture propagation. The purpose of the work described here was to perform modifications to a prototype seismic monitoring tool to address some of the shortcomings that were identified during past deployments. Additionally, advances in high temperature components have yielded new technologies that can be integrated in the seismic tool.

Chapter 2. LITERATURE REVIEW

2.1 Enhanced Geothermal Systems

Geothermal energy consists of thermal energy stored in the earth's crust. The natural occurrence of hydrothermal reservoirs is limited, but with the advent of enhanced geothermal systems, engineered reservoirs can be created for energy production. Enhanced geothermal system reservoirs are made by drilling wells into the hot rock where a stimulation process creates fractures in the rock. The fractures created enable a fluid (water) to flow between an injection and production wells. As fluid flows along permeable pathways, it is heated by *in situ* heat (heat obtained through direct contact with the hot rock) and pumped back to the surface through production wells. At the surface, the heated fluid is used to drive a turbine creating electricity. Upon leaving the power plant, the fluid is returned to the reservoir through injections wells completing the cycle. If the plant uses a closed-loop cycle to generate electricity, none of the fluids vent to the atmosphere resulting in no greenhouse gas emissions (Jefferson W. Tester, 2006). A cutaway diagram of an enhanced geothermal system is shown in Figure 2 (U.S. Department of Energy, 2008).

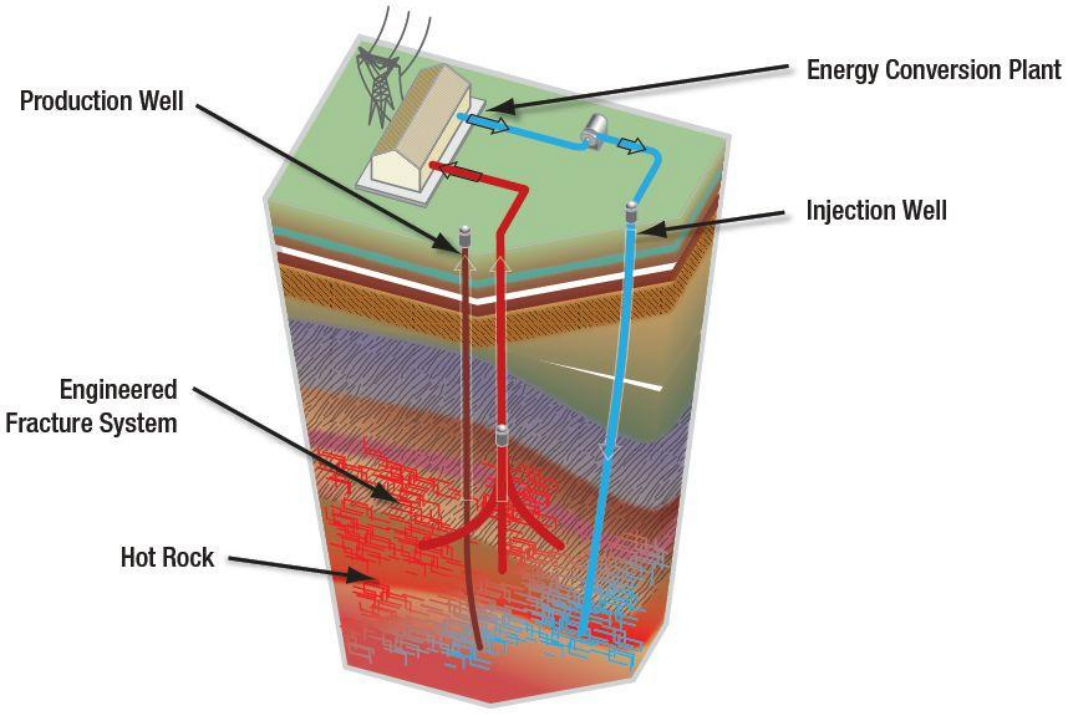

Figure 2: Enhanced Geothermal System Cutaway Diagram

2.2 Geothermal Stimulation Processes

There are two primary stimulation processes for creating the fractures required in geothermal power production: hydraulic fracturing (fracking) and hydroshearing.

2.2.1 Hydraulic Fracturing

Geothermal extraction from underground reservoirs is accomplished through drill holes. These drill holes allow hot, subterranean water to travel upwards while turning into steam. When the steam reaches the surface, it is used to power turbines that generate electricity. Drill holes are traditionally vertical, but the advent of horizontal boring has enabled more options for geothermal extraction.

The geology of the enhanced geothermal system location determines whether vertical or horizontal wells are used. At greater depths, high lithostatic pressure levels limit the extent of open fractures which serve as flow paths, and enhancement may be required to enable fluid circulation. The fractures are typically held open by use of sand or other proppants, physical media that is injected with the fracking fluid that subsequently props open the new fractures against geologic stresses. Horizontal drilling techniques may be used to access the target formation.

Fracking is accomplished by over-pressuring the bore-hole to the extent that the physical containment capacity is exceeded. When exceeded, the pressurized fluid will either open the rock mass along pre-existing seams or weaknesses, or exceed the combination of rock mass tensile strength and lithostatic confining stress. These fractures will propagate, following paths of least resistance. The direction and distribution of fracture pattern will be controlled largely by *in situ* stresses and discontinuities, generally propagating parallel to the principal stresses (Environmental Protection Agency, 2004). Fracking operations are shown in Figure 3 (U.S. Department of Energy, 2012).

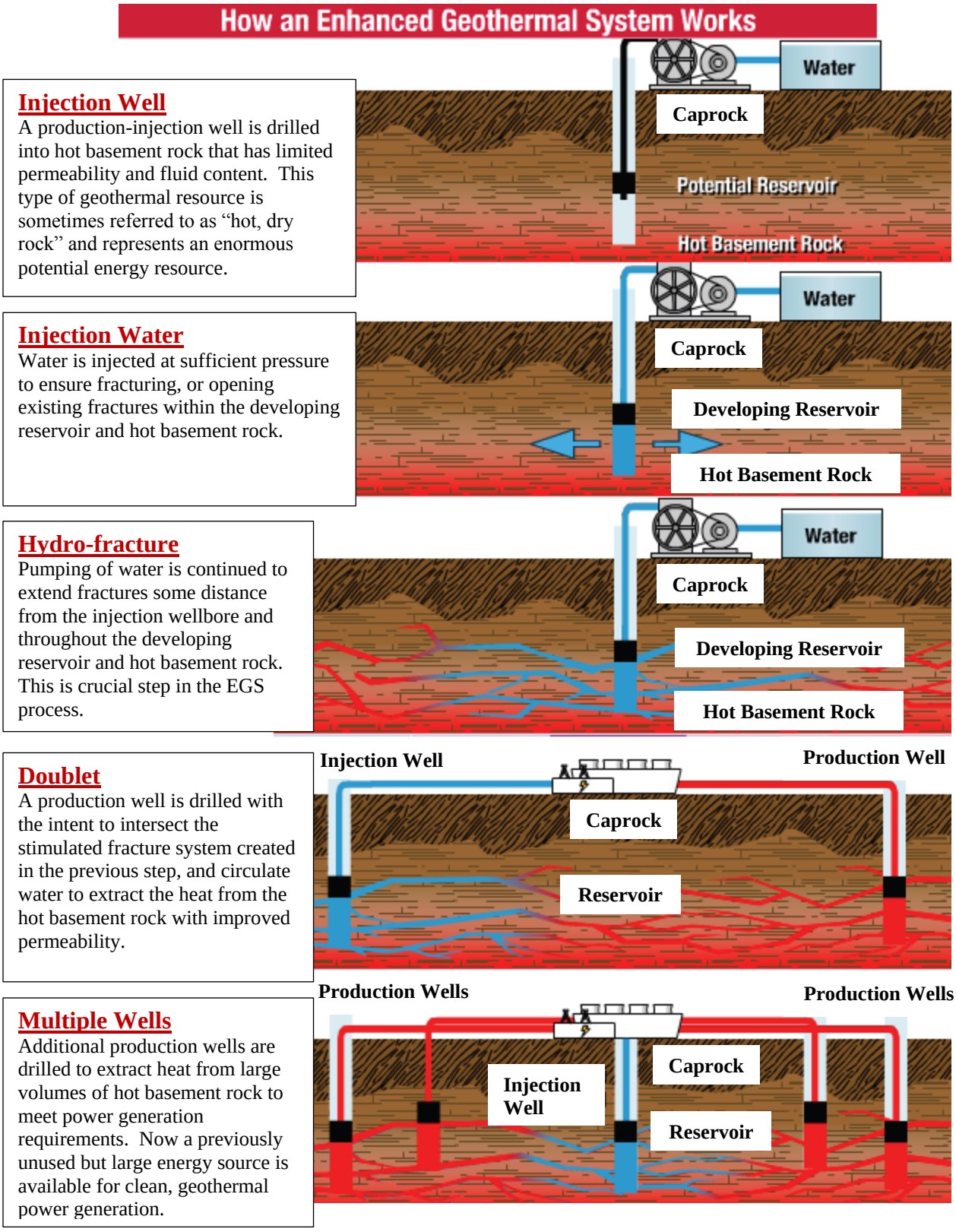

Figure 3: Enhanced Geothermal System Fracturing Operations

2.2.2 Basics of Hydroshearing

Hydroshearing is a relatively new method for producing fractures in impermeable rock. Hydroshearing occurs when friction is reduced on natural rock fractures by increased water pressure, which allows the fracture walls to slide past each other. The pressures required for this process are much less than those needed to break, or frack, the rock. Further, hydroshearing does not require proppants because the small fractures created will remain slightly open do to the irregularities on the fracture walls (AltaRock Energy, 2012). Because of natural variations in rock mass physical properties, structures, and local and regional stress patterns, both fracking and hydroshearing operations cannot be directionally "controlled" in the same sense that bore-hole drilling is controlled. In the well bore, stimulation operations may be preceded by explosive shape charges that pierce the bore-hole casing and cement liner (American Oil and Gas Historical Society, 2011). These piercing operations can be controlled with reasonable precision with respect to position and orientation in the hole, but the resulting fractures must be monitored during the stimulation process to know location and extent.

2.3 Seismic Monitoring

Micro-seismic monitoring tools are used to monitor the fracture creation process by recording the seismic activity in real-time. By locating micro-seismic events associated with the fractures, it is possible to determine the geometry of a fracture. Micro-seismic activity is measured using arrays of tools positioned in nearby observation wells. The data is then compiled and rendered to depict the effectiveness of the fracking or hydroshearing as shown in Figure 4 (Lawrence Berkeley National Laboratory, Earth Science Division, 2012).

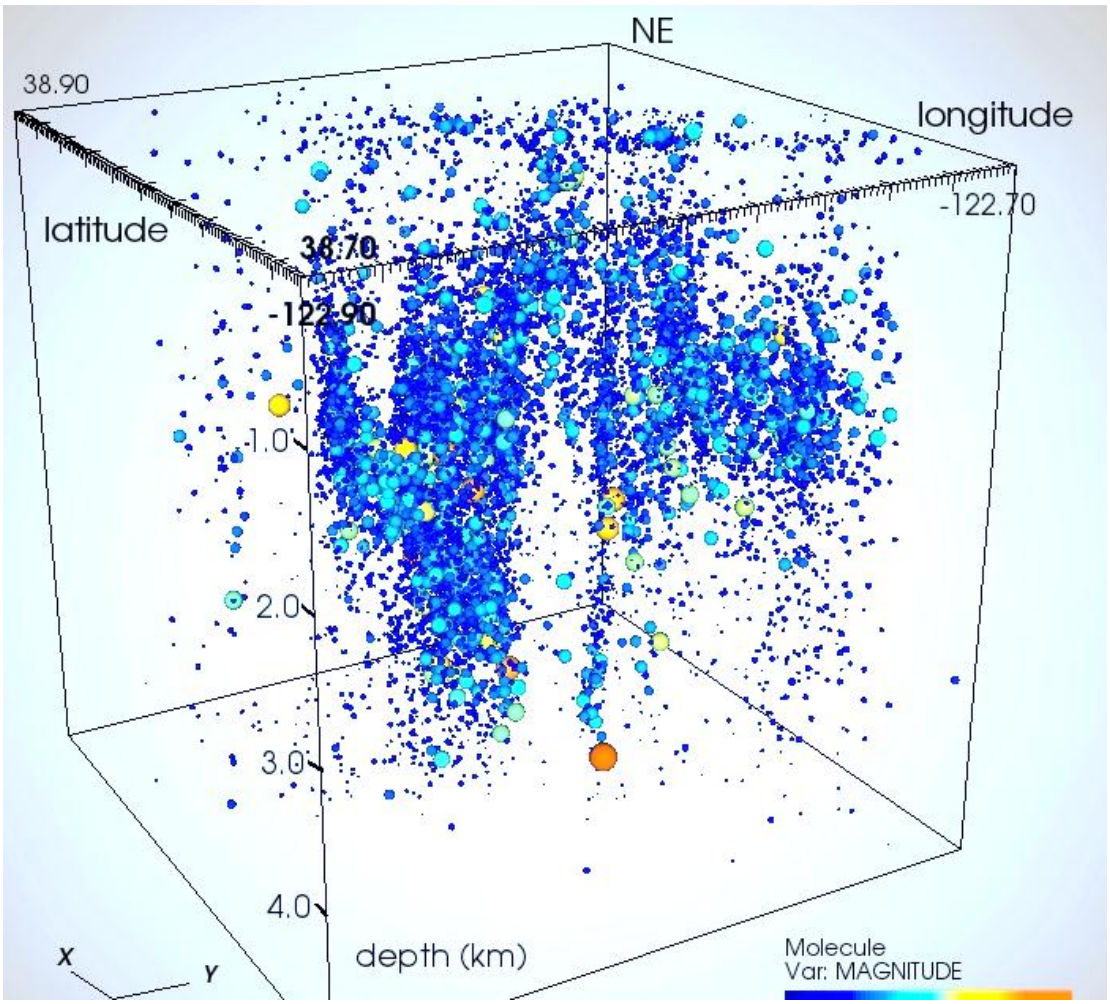

Figure 4: Seismic Monitoring Data Plot

Figure 4 is based on the seismic data collected at The Geysers geothermal field in northern California, the largest single geothermal field in the world. This data is related to the production and injection phases and used as a general indicator of fluid paths and reservoir response. Each location where seismic activity occurred was represented by a sphere, color-coded and sized depending on the magnitude. (Lawrence Berkeley National Laboratory, Earth Science Division, 2012). By closely monitoring this process, the micro-seismic event map reveals the relative size, location, and orientation of the fracture system. This information can help assess stimulation effectiveness and provide information necessary to properly create a geothermal reservoir. In addition, reservoir monitoring of the micro-seismic activity can provide information on reservoir performance and evolution over time (Henfling, Greving, Maldonado, Chavira, & Uhl, 2010).

2.4 Current Technologies

Most micro-seismic monitoring tools used within the oil and gas industry follow the same basic design. The sensors used to monitor the seismic events must be coupled securely to the bore-hole wall to ensure reliable data. The coupling force is generally provided by the use of a coupling arm which extends from the tool securing the device to the bore-hole wall, as shown in Figure 5 (Mitcham Industires, Inc., 2012).

Figure 5: Sercel Downhole Siesmic Array Systems

The securing of the device is crucial to the tools ability to record accurate seismic data. Because the same information sought in the oil industry is necessary for enhanced geothermal systems, a similar tool must be developed with appropriate modifications to survive the environments where geothermal energy exists.

Chapter 3. REQUIREMENTS, CONSTRAINTS, AND SYSTEM DESIGN

3.1 Environmental Requirements and Constraints

The seismic monitoring tool will be exposed to severe environments that drive the design parameters of the tool. These same environments preclude application of standard engineering

practice for many of the components in the systems that have to be deployed. These environments are characterized below in terms of chemical or physical attributes.

3.1.1 Physical

The remote environment where the micro-seismic monitoring tool will be used includes high temperatures, pressures, and corrosive fluids. Depending on the geothermal site, the tool can see temperatures reaching up to 300 - 400°C (572 - 752°F), (Asmundsson, Normann, Lubotzki, & Livesay, 2011). This is the primary factor when electronic components are selected. When constructing a high temperature device, the limiting factor will be the least temperature tolerant part which limits the selection of components. The tool is often submerged in brine or drilling mud, which creates a large pressure on the housing of the tool. Depending on the fluid density, the tool can see pressures up to 1,000 bar (15,000 psi), (Asmundsson, Normann, Lubotzki, & Livesay, 2011). The tool has to be built to withstand the pressures as well as keep the liquid from entering sensitive mechanical and electrical components which are completely sealed while in operation. The tool has to be relatively small and has a unique form factor of being cylindrical with a large length-to-diameter ratio. This affects the design of the electronics, further limiting the options for controlling the motor and data collection methods. In addition to these physical conditions, the tool has to be resistant to attrition that accompanies being handled around well field operations including shock, bump, and vibration.

3.1.2 Chemical

The tool is submerged in high temperature, electrically conductive and corrosive brines. High mineral content of the brine means all mechanical components must be designed to prevent or withstand mineral build-up. The brine is frequently boiling and can have varying ranges of acidity. Geothermal brines contain a high concentration of dissolved, ionized mineral salts – mainly chlorides and sulfates, which are highly corrosive. Various corrosive agents and processes can occur in geothermal brines including the production of hydrogen sulfide, carbon dioxide, and ammonia (Valdez, Schorr, & Arce, 2006). The hydrogen sulfide can cause brittleness often referred to as hydrogen embrittlement. Hydrogen embrittlement can damage the tool housing and the cables used for data communications to the surface (S.P. Lynch, Defence Science & Technology Organisation, 2007). Based on the brine composition, materials used to build the tool, and monitoring duration, deposits of arsenic, cyanide, or cadmium can form a

scale on the tool. Special care may be required when removing the tool from the bore-hole due to these toxic substances.

3.2 System Conceptual Design

To survive the environment described, the creation of a monitoring tool that integrated a mechanical system, which was monitored and controlled by an electrical system, all concurrently controlled by supporting software was required. The tool is lowered and operated in bore-holes of various diameters reaching depths of up to 1,500 m (4,921 ft.). The operational depth limit is primarily dependent upon data transmission lines. At distances greater than 1,500 m (4,921 ft.), signal distortion can occur when using wire-line (a combination of support cable and electrical data cables) resulting in faulty data. When the tool is secured at a specified depth in the bore-hole, data is collected and sent to the surface where it is recorded.

From the system design specifications, the high temperature seismic monitoring tool was adapted and built with specific requirements to meet design constraints. To secure the seismic sensor to the bore-hole wall, a mechanical coupling arm is extended by the tool until the desired force is applied. The monitoring electronics, located within the body of the tool, can monitor and collect seismic activity data and transmit the information to the surface where it is recoded. Figure 6: *Seismic Monitor Tool Deployment*, shows the seismic tool deployment in a bore-hole. Multiple tools are planned to be set in an array around a given area.

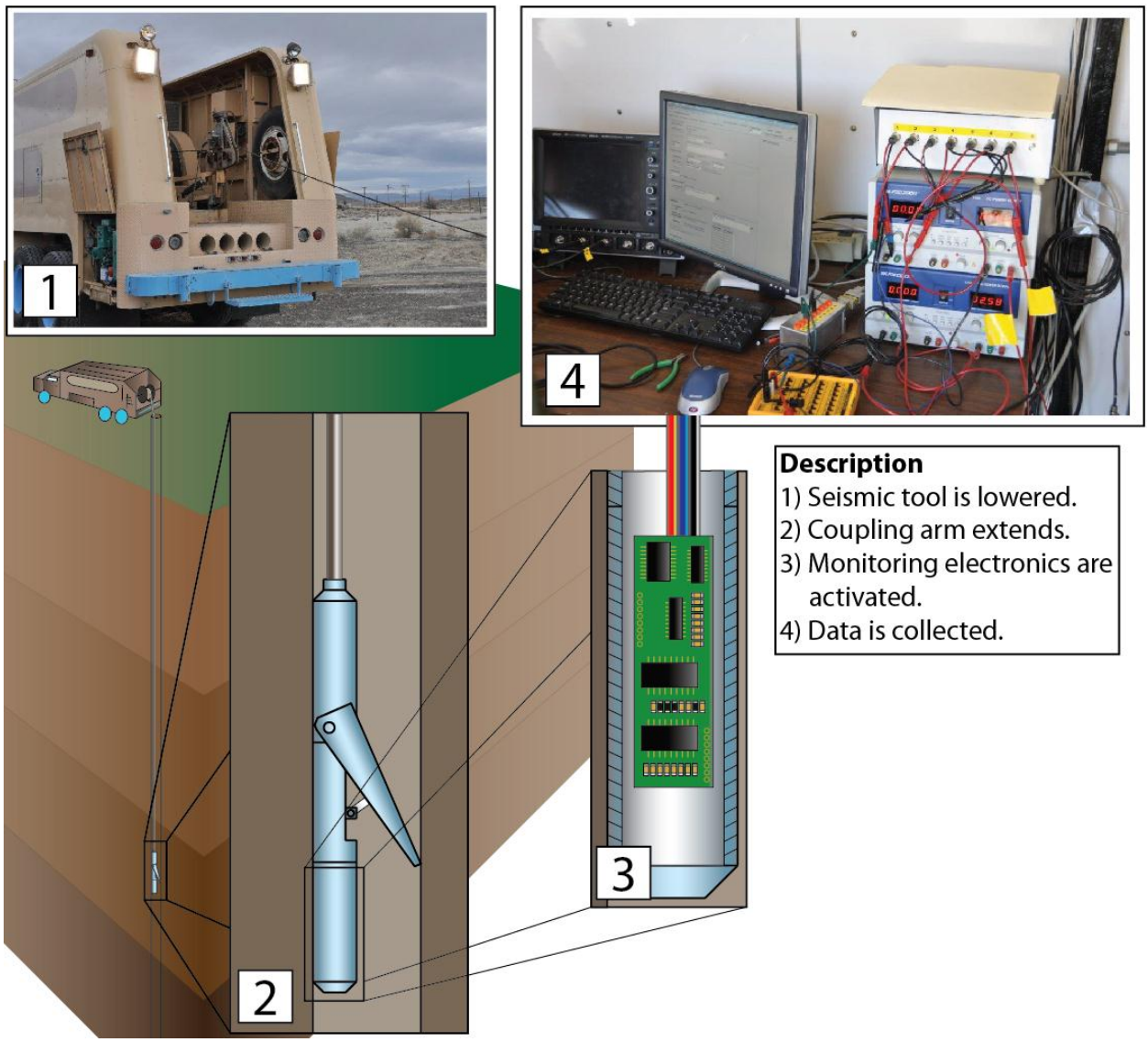

Figure 6: Seismic Monitor Tool Deployment

As depicted in Figure 6, the tool is lowered to the pre-determined depth by a logging truck which uses a winch. Once the tool has reached the appropriate depth, the coupling arm extends, creating a compressive force between the bore-hole wall and where the seismic signal is sensed. These vibrations will be recorded by accelerometers within the tool to measure seismic vibrations. The data is captured and sent to the surface where it is stored. Once the data is collected, the tool is removed from the bore-hole.

Chapter 4. SYSTEM DESIGN SPECIFICATIONS

To meet the requirements and constraints noted in Chapter 3, design specifications were established.

4.1 Conventional Technology

The prototype seismic tool design was based upon proven technologies utilized by the oil and gas industry. The tool required modifications to work at the extreme environments including a new motor and high temperature electronics.

4.2 High Temperature Adaptations

Using design parameters set in Chapter 3, a base-line prototype seismic monitoring system was designed and built in 2010. Since then, various components have been redesigned and adapted to further the prototype development. The initial prototype seismic monitoring system was comprised of three basic elements: 1) a mechanical system that creates the coupling between the sensors and the bore-hole wall, 2) an electrical system that controls the motor, which controls the mechanical system, and 3) an operator. During previous applications, deployment of the tool was controlled by the operator at the surface who would monitor the data and make adjustments.

4.2.1 Mechanical System Specifications

The mechanical system design was modified to work in an operational temperature of 210°C. To secure the seismic tool to the bore-hole wall, the required force was first characterized. It was determined that the coupling arm force was proportional to the tool weight, at a minimum rate of the coefficient of friction between the tool and bore-hole wall. The prototype was built using stainless steel, weighing close to 27.2 kg (60 lb.) and the basic rule of thumb was to ensure a radial coupling force between the tool and the bore-hole of five times the tool weight. Based on the coupling arm force metric, the minimum required extension force was determined to be approximately 1,334 N (300 lbf.). The required coupling arm force was set at 1,779 N (400 lbf.) to add a factor of safety to the coupling force and to accommodate the cable weight used to lower the tool. To provide the driving force to the coupling arm a motor resistant to high temperature was required and needed to be isolated from the environment. Additionally, the coupling arm mechanism would be exposed to high pressures and corrosive brines.

4.2.2 Electrical System

The electronic system was based upon available technology which is limited in high temperature environments. A controller was chosen to meet the requirements of the tool based on six constraints: 1) build size, 2) availability, 3) operational temperature, 4) duration of operational time at temperature, 5) computational speed, and 6) cost. Build size and availability were deemed design constraints because of the limited space and time to acquire them. A controller board that is located down-hole in the tool has to fit within the available space. If the controller was physically too large or not readily available, it was not chosen to investigate at the component level. The minimum operational temperature and duration requirements were set at 210°C for 1,000 hours. The data collection system at the tool level was required to have high computational speed, ensuring the accelerometer data could be reliably collected. Cost was considered as a comparator driven primarily by the costs of the support materials needed to use the controller.

4.2.3 Operational System

To deploy the prototype tool, an operator would lower the tool until the required depth was reached and the coupling arm could be extended. During coupling arm extension, the operator would monitor the current provided from the power supply until a pre-determined current was measured which indicated contact with the bore-hole wall. Reliance on the skill, mental alertness, and responsiveness the operator could yield errors in which the coupling arm's shear pin capacity could be exceeded, causing it to break. The tool would then need to be brought back to the surface for repair before redeployment and this scenario was to be avoided. To limit the potential for operator error during the extension process, an automated controller system integrated into the tool is required.

Chapter 5. SEISMIC MONITORING SYSTEM DESIGN MODIFICATIONS

To meet specifications defined in Chapter 4, each of the three basic elements were revaluated: 1) the mechanical system, 2) the electrical system, and 3) controlling software.

5.1 Mechanical System Design

The prototype seismic tool was constructed with stainless steel (type 316 LC) which would allow the tool to work within the conditions described in Section 3.1. A mechanical power source was required to supply the force to the coupling arm. Previous hardware limitations resulted in the use of a stepper motor which produced additional challenges while implementing monitoring operations. Advances in high temperature components have resulted in the production of DC motors that meet the temperature requirements for operational use and can be integrated in the seismic tool. In comparison to a DC motor, a stepper motor requires multiple signals and additional electronics to run which increase the overall dimensions and weight of the tool. The benefits of using a DC motor within the tool include: 1) easier to control, 2) can be simultaneously used with multiple tool systems within the same bore-hole to create a seismic array, and 3) less controlling circuitry potentially reducing tool size. To further ensure corrosive brines could not enter and degrade the system, the complete mechanical drive system was immersed and sealed in an oil reservoir.

5.2 Electrical Design

Three controllers were compared to determine the best option for controlling the seismic tool. The digital control options compared were the ARM 7 (high temperature version from Texas Instruments), 8051 (high temperature version from Honeywell), and Field-Programmable Gate Array (FPGA). During the process for selecting the motor controller, Table 1 was developed to compare the various technologies, originally produced by Frank Maldonado and Scott Lindblom. An explanation of the metrics required for the selection matrix is provided in Appendix A.

Table 1: Digital Controller Selection Matrix

Digital Control Options for Motor Controller							
Comparisons (listed below)	ARM 7	8051	FPGA	Note: Costs were driven by additional components needed to operate controller. (ADC, EEPROM, Memory, Power Source, etc.)			
Operating Temp. (°C)	200	225	240				
Duration (hrs)	1000	43800	3000				
Computation Speed	7	3	10				
Cost Approx. ($)	6000	4000	2800				
Constraints		**ARM 7**		**8051**		**FPGA**	
BUILD SIZE		**Yes**		**Yes**		**Yes**	
AVAILIBILITY		**Yes**		**Yes**		**Yes**	
	Weight (%)	**Score**	**Weighted Score**	**Score**	**Weighted Score**	**Score**	**Weighted Score**
Operating Temp. (°C)	**50**	0.00	0.00	0.63	0.31	1.00	0.50
Duration (hrs)	**10**	0.00	0.00	1.00	0.10	0.05	0.00
Computation Speed	**20**	0.57	0.11	0.00	0.00	1.00	0.20
Cost ($)	**20**	0.00	0.00	0.63	0.13	1.00	0.20
TOTAL	**100**		**0.11**		**0.54**		**0.90**

After comparing the three options, the FPGA was selected to control the system. To reduce reliance on the operator for the seismic tool's coupling operations, an integrated solution was required to measure the force within the existing design. Traditional methods, including the use of externally placed strain gauges or load cells, were not practical as the harsh conditions would eventually destroy the sensor. The method used for this application was to measure motor electrical current, an inexpensive and structurally uncompromising method for determining load. This could be done because motor power consumption is directly and linearly related to motor force which creates the coupling force with the bore-hole wall. To measure current, a current sensing resistor (referred to as a shunt resistor) was required. The voltage drop seen across the shunt resistor (as a function of current) could be read by the controller and the supporting code could use this value to control the motor based on the coupling force requirements (Zhen, 2012).

5.3 Software Design

To control the FPGA controller required the use of VHDL (a hardware description language used to describe digital systems). The key advantage of using an FPGA is the ability to conduct computational processes in parallel versus in series. Operating parallel processes results in a greater sampling of data over more channels (Chu, 2006). The seismic data collection unit is operated from the surface, so having the capacity to transmit large volumes of data is necessary. A flow diagram for developing the software is shown in Figure 7.

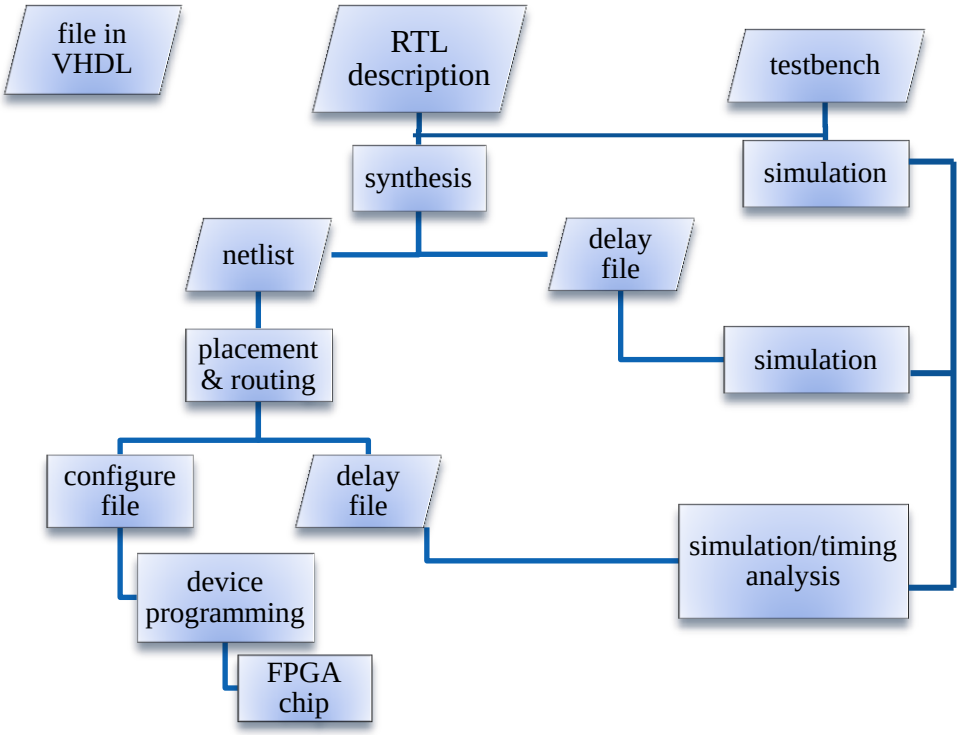

Figure 7: FPGA Controller Code Structure

Controlling the coupling arm motor required obtaining analog data from the shunt resistor and then converting it to a digital signal, where it could be utilized by the program. When the data was read it was compared to a threshold value (a conditional value which would either run or stop the motor). If the force was below the desired requirement, the motor would continue to run until the required force was met as indicated by the voltage across the shunt resistor. This process ensured proper coupling of the tool to the bore-hole wall. The code followed the logic flow shown in Figure 8.

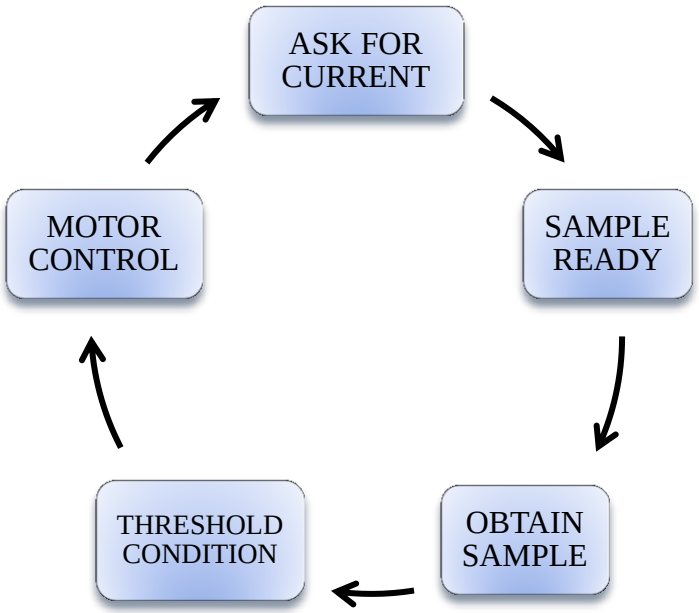

Figure 8: Current Sensor Code Sequence

In order for the coupling arm to apply the correct force, the threshold values must be determined based on the bore-hole diameter because the mechanical advantage of the motor output is a function of arm extension.

Chapter 6. COMPONENT AND SYSTEM TESTING SEQUENCE DESIGN

Testing of the system was conducted in three phases to develop the needed functionality of each subsystem including the: 1) mechanical system, 2) the electrical system, and 3) the fully integrated system. Chapter 7 *Phase 1: Component Testing* describes procedures and results from the high temperature testing done on the components. Chapter 8 *Phase 2: Electro-Mechanical System Test* describes the procedures and results from testing the coupling arm force and current sensor. This section includes calculations done after the initial characterization tests were conducted. This initial test measured key outputs to enable selection of a proposed gear box and electrical current sensor modifications. Based on the initial test, new control values were integrated into the design and the test sequence was repeated to confirm proper functionality. Chapter 9 *Phase 3: Integrated Software-Electro-Mechanical System Testing* describes the testing of the integrated system with a fully functioning control unit providing feedback between the coupling arm and motor drive.

Chapter 7. PHASE 1: COMPONENT TESTING

Phase 1 objectives were to verify that both the DC motor and the motor torque sensor worked at high temperature (up to 210^{o}C for several hours). The motor torque sensor was comprised of an electrical current sensor because motor torque was found to correlate well with electrical current. Since the torque sensor design relied on the operational success of the DC motor at high temperature, the first test conducted was on the motor. If the motor failed, the current sensing modifications would be conducted based on different motor parameters. Once motor selection was determined, the electrical current sensor was designed and built. The components used to create the electrical current sensor were based on proven technology and well characterized components, so the primary goal was to measure component performance as a function of temperature. These tests were facilitated with the use of a programmable oven. Upon successful completion, both components could be integrated to the existing hardware.

7.1 Supporting Equipment

Based on the testing requirements, the equipment used was categorized as being either physical support equipment or diagnostic equipment. All testing was conducted in a laboratory setting.

7.1.1 Physical Support Equipment

Component characterization at high temperature required the support items listed in Table 2 and shown in Figure 9.

Figure 9: Component Test Physical Support Equipment

Table 2: Component Testing Physical Support Equipment

Item #	Item Name	Description
1	Fisher Scientific Isotemp Oven 851F	Oven used to simulate temperatures of operational environment (vented).
2	Sorensen XHR 60-18	24V DC power supply used to supply power to DC motor.
3	Agilent E3612A	5V DC power supply used to power current sensor operational amplifier.
4	KEITHLEY-2400	Current source for current sensor testing.
5	Globe Motor 5A4445	DC motor.
6	One-Piece Rigid Coupling	Rigid coupling used to connect motor to shaft for motor testing.
7	1/4in Drive Shaft	Extension of Drive Shaft used for motor testing.
8	Unistrut	Mounting brackets used to support motor test stand and mounting motor in oven.
9	Steel motor mount	Steel plate machined to house motor for in-oven testing.
10	Ball Bearing	Simulate frictionless surface when load was applied to drive shaft (preventing drive shaft flex).
11	Pulley (6in radius)	Increase lever arm on motor shaft to simulate a heavier load.
12	Pulley (2in radius)	Guide nylon string.
13	32 ounce weight	Provides a load on the motor.
14	Rigid ™ Support Frame	Provide support to complete tool when tested under load cell.
15	Soldering Iron and Solder	High temperature soldering iron used to construct current sensor.
16	Teflon Coated Wire	Used in construction of current sensor.

7.1.2 Diagnostic Support Equipment

The equipment used to measure and record data for high temperature component testing is listed in Table 3 and shown in Figure 10.

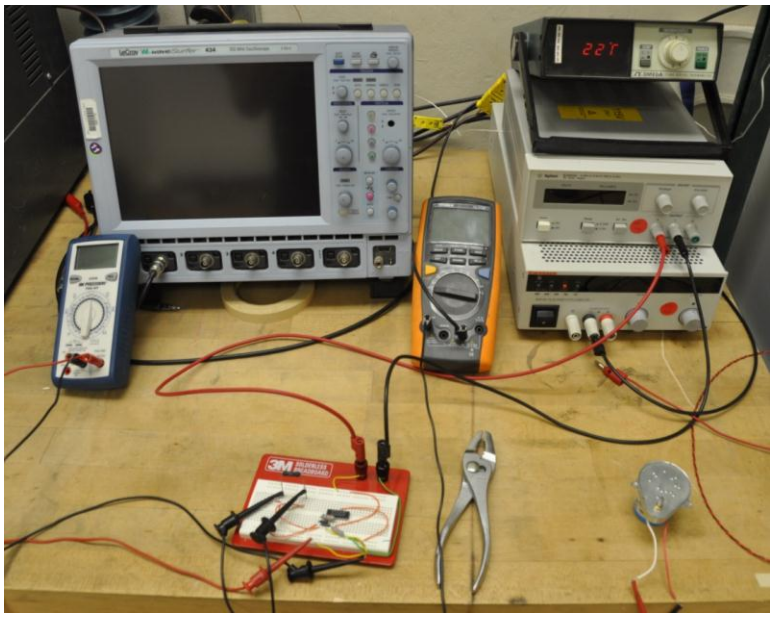

Figure 10: Component Test Diagnostic Support Equipment

Table 3: Component Testing Diagnostic Equipment

Item #	Item Name	Description
1	BK Precision 2707B	Voltage meter used to measure voltage from current sensor output.
2	TENMA 72-7732	Current meter placed in line with motor to verify current sensor measurements.
3	OMEGA 2168A	Digital thermometer display to verify oven temperature and motor temperature.
4	K-type Thermocouple	Thermocouple used with digital thermometer.
5	MTS Load Cell	Obtain force produced by the motor within tool.
6	Load Cell Support Software	Captured load cell data, voltage reading from current sensor, and motor temperature.
7	LMC660CN	Low Temperature op-amp used to build a test current sensor.
8	HTOP01	High Temperature op-amp used to build production current sensor.
9	Resistors	Supporting circuitry for building current sensor.

7.2 High Temperature Motor Test

The first component tested was the motor. Since the motor had been custom made, there was no data sheet provided to characterize the performance. The only information known was that the motor required a 24 volt power supply and had a gear reduction ratio of 524.6 to 1. Based on the visual appearance of the motor, a data sheet was selected from possible motor specification data

sheets made available by the motor manufacturer. From the selected data sheet, the known gear reduction ratio was to produce an output torque of 2.58 Nm (366 oz-in.). Testing of the motor involved applying a load on the motor at half motor capacity. To measure the operational capacity, a pulley was selected to increase the lever arm of the motor. A 15.24 cm (6 in.) pulley and 0.91 kg (32 oz.) weight were used to apply the desired load. The load applied by the weight would result in the motor operating at 1.36 Nm (192 oz-in.) of torque (slightly above half capacity) neglecting the forces of friction. The test set up is shown in Figure 11.

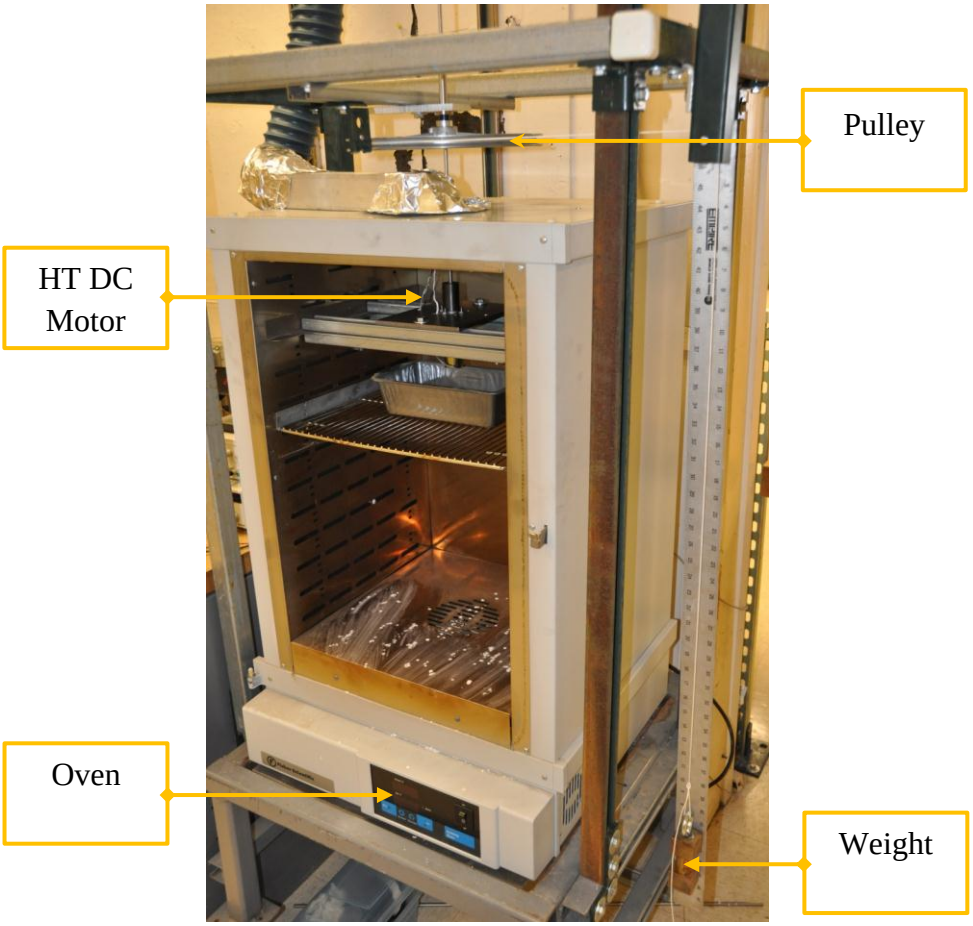

Figure 11: High Temperature Motor Test Setup

7.2.1 Procedure for Testing Motor

The test was conducted by supplying 24 volts directly to the motor, which resulted in the lifting of the weight. While the motor was in operation, the following information was obtained manually on data forms: 1) time, 2) temperature, 3) current, and 4) voltage-out based on the current sensor. The test was conducted following the testing procedure located in Appendix B**.**

The voltage-out from the initial trial current sensor was done with a low temperature circuit, which was placed outside the oven. Figure 12 shows the initial low temperature current sensor which was supplied 5 volts to amplify the voltage-out signal produced by the shunt resistor (highlighted in orange).

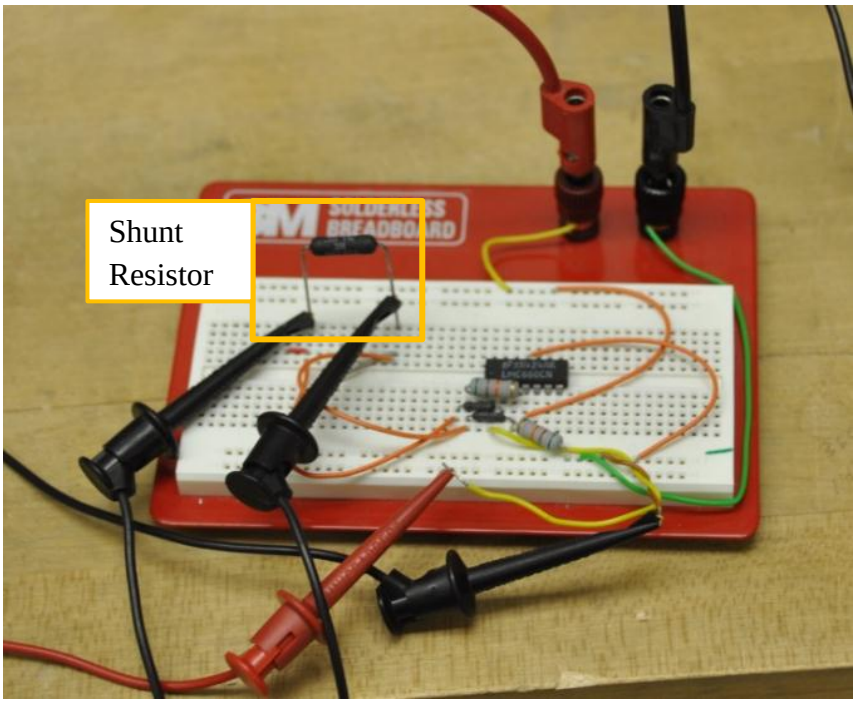

Figure 12: Initial Trial Current Sensor (Low Temperature)

The description of the resistor selection procedure for the torque sensor is in Appendix C. The design schematic and support documentation for the low-temperature sensor is in Appendix D.

7.2.2 Results

Figure 13 shows the current required by the motor to apply a constant torque when supplied 24 volts at various temperatures.

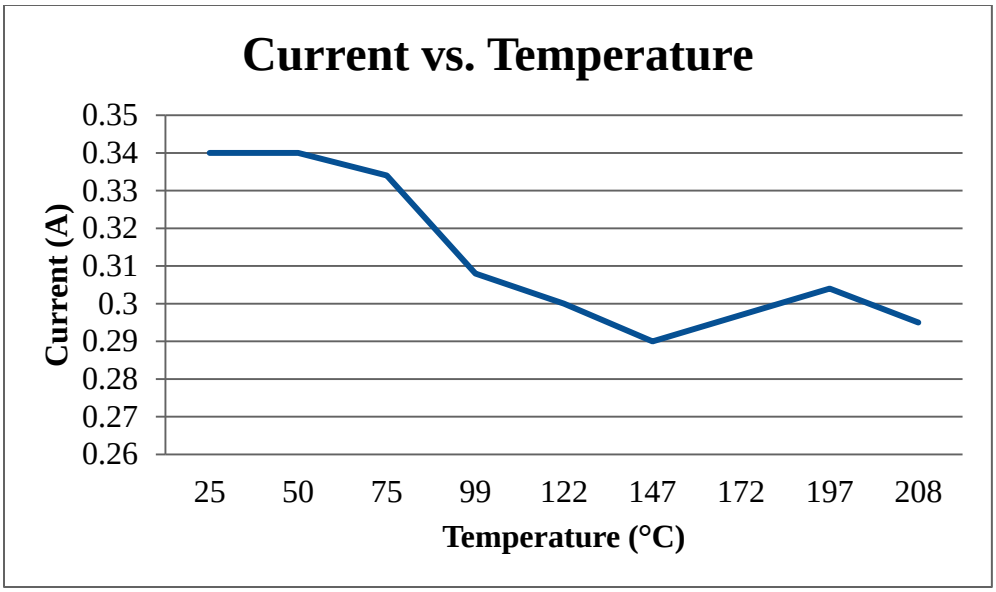

Figure 13: Motor Current as a Function of Temperature

7.2.3 Performance/Conclusions

The motor survived the high temperature test so the resistor values could be determined for the high temperature current sensor. As shown in Figure 13, as temperature increased, the current required to lift the weight decreased steadily. The concluding thought was that as the temperatures increased, the resistances (both mechanical and electrical) were decreasing which would result in less energy required to run the motor. When the motor was lifting the load and power was removed, the weight would stop immediately throughout all temperatures tested. However, when power was removed from the motor while the weight was being lowered, at temperatures greater than 125°C, the motor failed to secure the load. With the high gearing ratio, this was a phenomenon that was not expected. A concern was that the motor might be driven backward when power was not applied. To test the static unpowered load capacity of the motor, upon completion of the first test, the weight was raised and power was removed. The following day, verification was done to allow the oven and motor to return to ambient temperature. The weight was still at the original location confirming the motor's ability to maintain the holding torque without power. With motor performance shown to be adequate, a motor torque sensor (based on motor current) could be designed and tested.

7.3 High Temperature Current Sensor Test

The motor current sensor utilized a single low value resistor, often referred to as a shunt resistor, to create a voltage-drop that could be measured. Resistor selection required knowing the maximum current the motor would use. Using the current to directly relate coupling arm force at the bore-hole wall required the current sensor to operate within a specific range to maximize the sensitivity of the torque measurement. To obtain the maximum current, the motor was run until it stalled, resulting in a maximum current of 0.92 A. Using this value, resistors used to amplify the signal by means of an operational amplifier were selected following the steps described in Appendix C. Once the values were determined, the sensor was built using high temperature components and placed in the oven as shown in Figure 14.

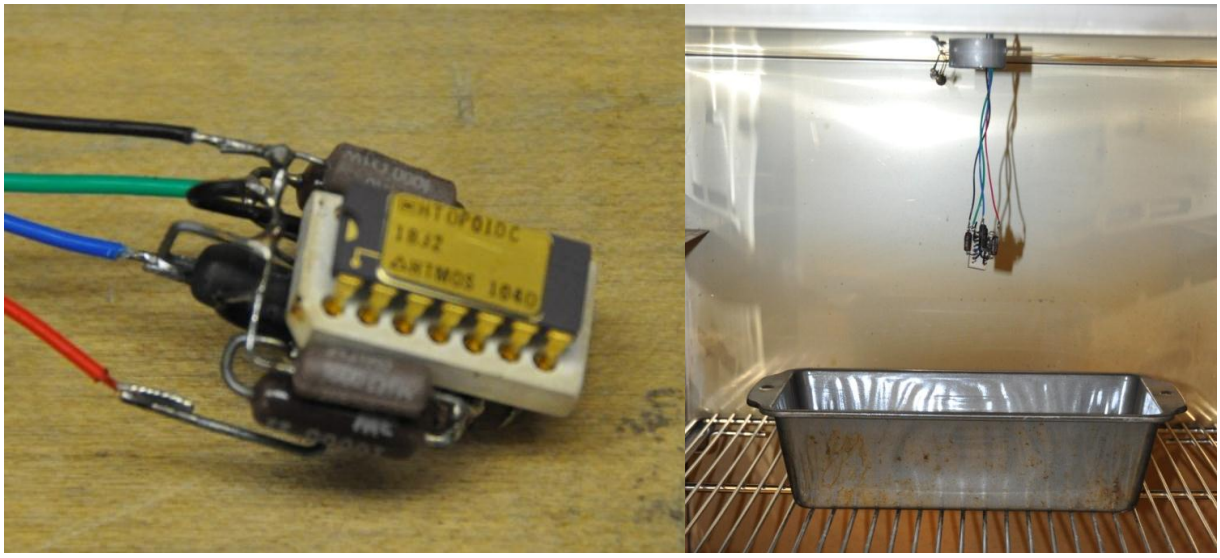

Figure 14: High Temperature Current Sensor (Left), Sensor in Oven (Right)

7.3.1 Procedure for Testing Current Sensing

High temperature current sensor testing was conducted in an oven and applying a current from a current source. When the current sensor was at the temperature desired, current was supplied at varying amplitudes (0.2, 0.4, 0.6, and 0.8 A) and the output voltage was manually recorded. The test was conducted following the testing procedure, in Appendix C.

7.3.2 Results

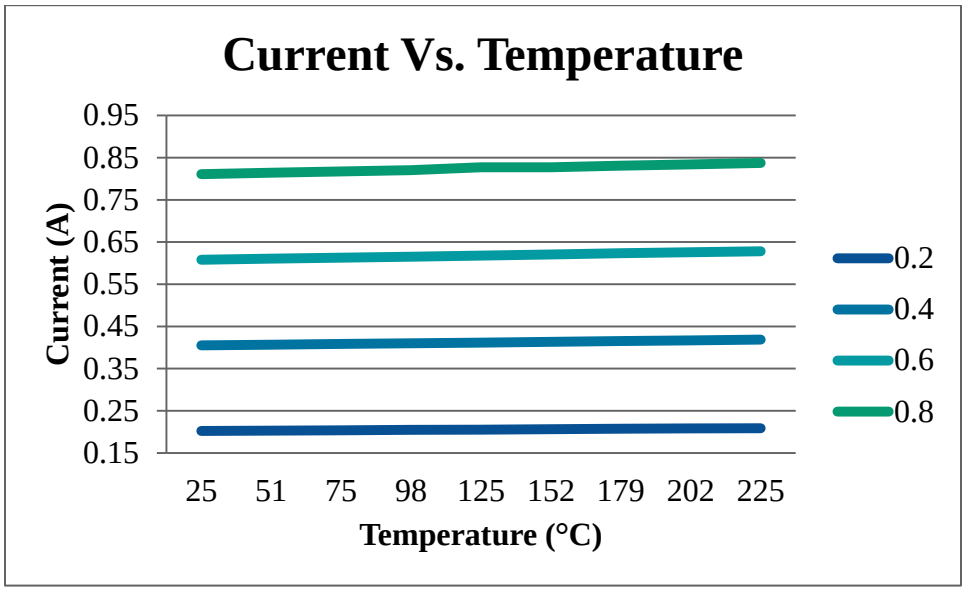

Figure 15: Current Sensor Performance based on Temperature

The data collected from the current sensor showed slight increases as a function of temperature but performed as required.

7.3.3 Performance/Conclusions

The electrical current sensor circuit survived the high temperature test as expected. The circuit was left at 210°C overnight to ensure total circuit temperature saturation. Based on the results shown in Figure 15, the voltage-out reading resulted in an accurate current estimate. Since all components would be exposed to the same heat source, fluctuations in resistance should be seen across all components, resulting in reliable results. This is due to the fact that the circuit gain relies on the resistance ratios, not absolute values. The percent error was a function of the temperature. Based on the data, the worst case occurred at the highest temperature with an error of less than 5% when comparing the measured current against the supplied current source. Since the system does not require a measurement with higher accuracy, the current senor will be used to estimate motor torque output. With both required components passing their respective performance criteria, installing the components within the seismic tool could proceed to verify coupling arm performance.

Chapter 8. PHASE 2: ELECTRO-MECHANICAL SYSTEM TEST

Phase 2 objectives were to correlate current as a function of force and verify motor performance within the tool. The motor would need to generate a force at the bore-hole wall of at least 1,779 N (400 lbf.) at all positions of coupling arm extension. With no information about the level of torque required to generate the coupling force, preliminary scoping tests were conducted to correlate motor torque to coupling arm force. In addition to gear reduction, torque produced by the motor would be amplified by a worm gear of unknown specification located within the tool housing. Phase 2 testing was conducted in two parts. Initial tests, described in Section 8.1 *Initial Electro-Mechanical System Test,* were done using parts and design based upon incomplete knowledge of motor current use, so the data collected did not fully characterize system performance. Using this preliminary data, calculations described in Section 8.2 *Intermediate Design Calculations Based on Initial Tests*, were performed to enable selection of better motor current sensor resistor and supplemental resistors for magnifying the signal. The final test was conducted as described in Section 8.3 *Final Electro-Mechanical System Test*, with components and equipment that provided an accurate characterization of system performance.

8.1 Initial Electro-Mechanical System Test

To benchmark the electro-mechanical system, a test was conducted to determine the forces that could be produced at the end of the coupling arm with the use of a hydraulic load cell. The data acquisition system used to record the load cell data could also monitor the corresponding current sensor as well as a temperature probe located on the motor.

8.1.1 Support Equipment

Testing required use of the equipment that is listed below and categorized as being either physical supporting equipment or diagnostic equipment. All testing was conducted in a laboratory setting.

8.1.1.1 Physical Support Equipment

Physical support equipment used to facilitate the electro-mechanical component testing is listed in Table 4 and shown in
Figure 16.

Figure 16 shows the seismic tool securely placed under the load cell with the coupling arm contact point directly under the load cell. A piece of wood was used to protect the load cell surface from any damage caused during the extension process. To secure the seismic tool to the load cell support structure, clamps were used to secure a v-block channel which held the tool. Two hose clamps were then placed around the tool and secured to a steel shaft.

Figure 16: Initial Electro-Mechanical Physical Support Equipment

Table 4: Electro-Mechanical Physical Support Equipment

Item #	Item Name	Description
1	BK Precision 1761 DC Power Supply	Triple output power supply. 24V to motor, 7V to FPGA board, 5V to current sensor.
2	Globe Motor 5A4445	DC motor.
3	One-Piece Rigid Coupling	Rigid coupling used to connect motor to shaft for motor testing.
4	Rigid ™ Support Frame	Provide support to complete tool when tested under load cell.
5	Seismic tool	Seismic tool body which houses the motor and coupling arm mechanics.
6	MTS Load Cell Frame	Support framework for load cell.
7	Clamps and v-block	Used to secure the seismic tool to the load cell test frame.

8.1.1.2 Diagnostic Support Equipment

Equipment for measuring tool performance data is listed in Table 5 and shown in Figure 17. Figure 17 shows the testing setup for the initial electro-mechanical testing. The power supply was replaced from the initial component testing as more supply voltage outputs were required.

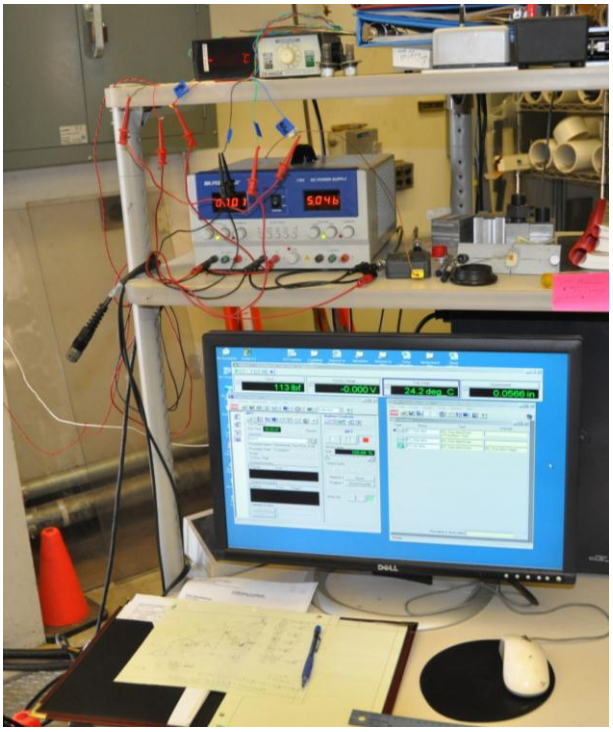

Figure 17: Initial Electro-Mechanical Diagnostic Support Equipment

Table 5: Electro-Mechanical Diagnostic Support Equipment

Item #	Item Name	Description
1	K-type Thermocouple	Thermocouple used with digital thermometer.
2	MTS Load Cell	Obtain force produced by coupling arm.
3	Data Acquisition System	Captured load cell data, voltage reading from current sensor, and motor temperature.
4	HTOP01	High Temperature op-amp used to build production current sensor.
5	Resistors	Supporting circuitry for building current sensor.

8.1.2 Procedure for Electro-Mechanical System Test

Before testing could begin, a new mounting bracket was designed to incorporate the motor to the seismic tool. During the high temperature motor component test, the original coupling adapters for coupling the motor to the load pulley were deemed unreliable because when applying torque

on the screws, the force caused one of the couplings to crack. Figure 18 shows the original coupling, with the crack circled in orange, next to its replacement.

Figure 18: Rigid Coupling Replacement

For reliability and repeated use, a larger coupling was chosen. To accommodate the larger coupling, longer spacers were built allowing the coupling adapter to attach the motor drive shaft to the worm gear drive shaft. Once all required parts were obtained and assembled, the outer-most tool casing was placed around the motor. To begin the electro-mechanical system test, the assembled tool was taken to a rock mechanics laboratory which has large load frames with load cells. The seismic tool was placed under a load cell with the tip of the coupling arm directly under the load cell sensor as shown in Figure 19.

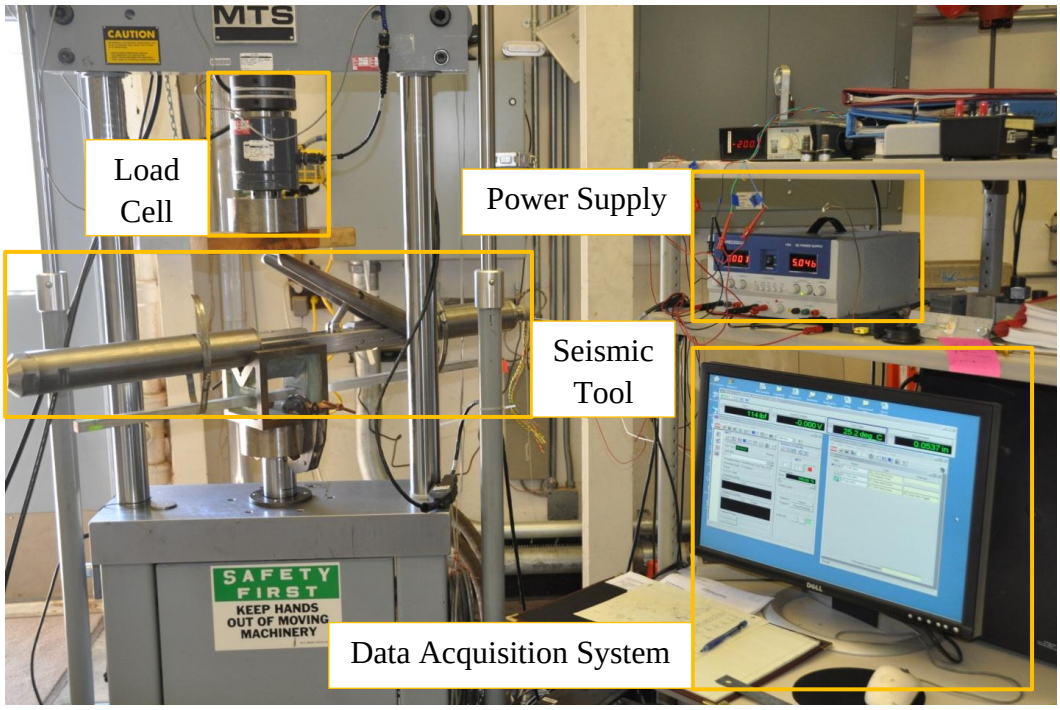

Figure 19: Initial Electro-Mechanical System Test Setup

When the motor was supplied 24 volts, the coupling arm would extend up until contact was achieved. While in motion, the data acquisition system would monitor and record the various measurements. The recorded data included: 1) time, 2) force applied by coupling arm, 3) electrical current measurements of the motor, and 4) motor temperature. Tests were conducted at predetermined coupling arm extensions which were all measured from the tool housing (where the tool would be in contact with the bore-hole wall) to the endpoint of the arm. Each of these extensions corresponds to a certain bore-hole diameter constraint. The test operating procedure is located in Appendix E.

8.1.3 Results

Testing was conducted at coupling arm extensions of 10.16 cm (4 in.), 12.70 cm (5 in.), 15.24 cm (6 in.), 17.78 cm (7 in.), 20.32 cm (8 in.), and 22.86 cm (9 in.) to simulate conditions in bore-holes of these same diameters. As shown in Figure 20, the motor did not produce the necessary force on the coupling arm, a limitation of the motor torque. At each extension, the motor was ran until it stalled.

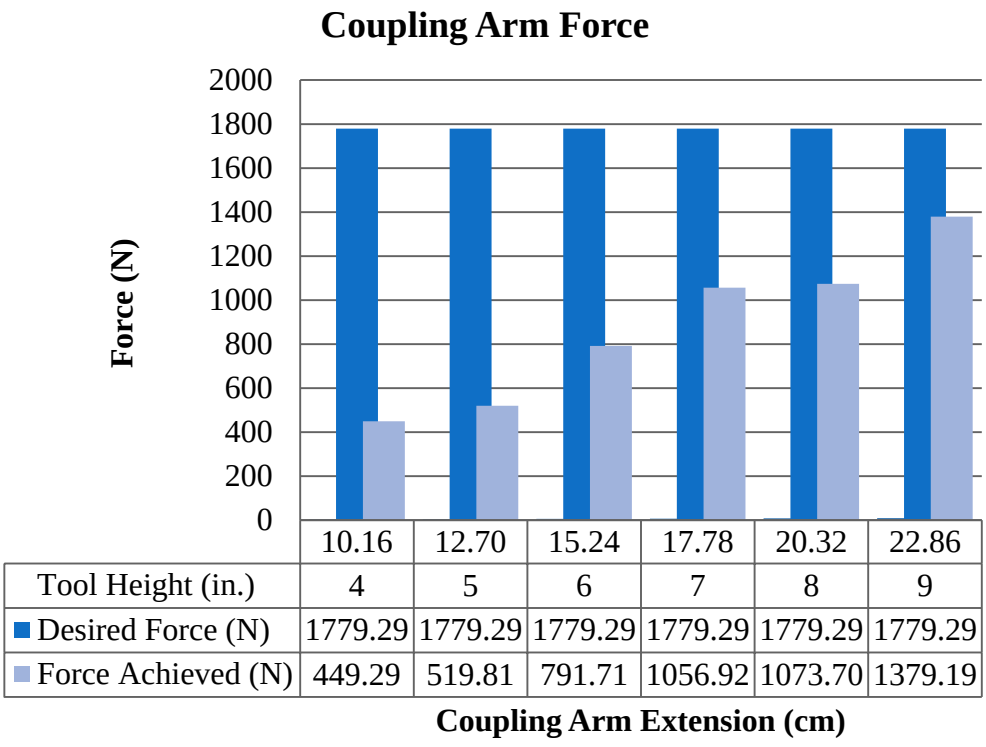

	10.16	12.70	15.24	17.78	20.32	22.86
Tool Height (in.)	4	5	6	7	8	9
Desired Force (N)	1779.29	1779.29	1779.29	1779.29	1779.29	1779.29
Force Achieved (N)	449.29	519.81	791.71	1056.92	1073.70	1379.19

Figure 20: Coupling Arm Force

As the force increased on the coupling arm, the current measured stayed at a constant value as shown in Figure 21. The current sensor values were exceeded at the point of motor stall.

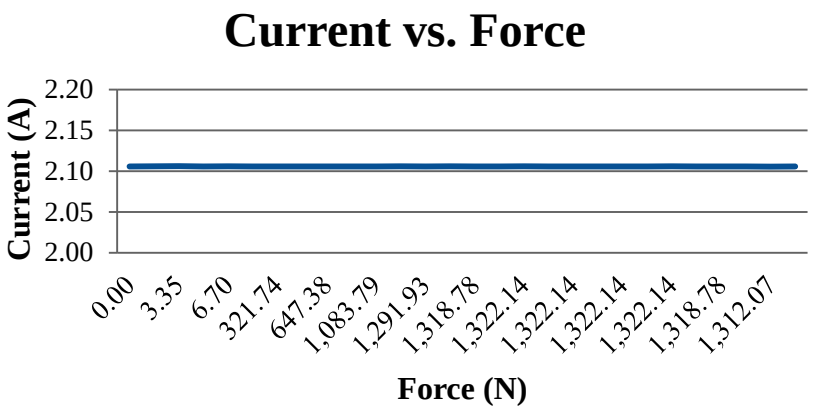

Figure 21: Current Voltage vs. Force at 22.86 cm (9 in.)

8.1.4 Conclusions

At the point of greatest mechanical advantage, the maximum force the seismic tool could produce was about 1,379 N (310 lbf.), less than the required force level. At positions of less mechanical advantage, output force was well below the required 1,779 N (400 lbf.) level. Prior to initial testing, there was no data determining the torque required within the seismic tool to produce the force needed. Based on the results of this test, supporting calculations were done to determine what torque the motor would need to produce to generate the required forces.

Initial component testing described in Section 7.3 *High Temperature Current Sensor Test*, were unintentionally and unknowingly current limited by the laboratory power supply at 0.92 A. This test series measured motor current to be as high as 1.5 A when using a different power supply. Because the electrical current sensor was designed for 0.92 A, subsequent tests would need to be conducted with a new set of operational amplification resistors to accommodate higher current levels.

8.2 Intermediate Design Calculations Based on Initial Tests

Because the motor and tool did not perform to the required specifications, the motor gear box and operational amplification resistors of the tool needed modification. Design calculations were performed to determine the gear reduction ratio to produce 1,779 N (400 lbf.) at the coupling arm

extension at the minimum bore-hole diameter or point of least mechanical advantage. If the tool could perform at this point, it would meet or exceed requirements at all other larger extensions or bore-hole diameters. Similarly design calculations were used to select appropriate resistors for the current sensor to allow correlation with extension arm force.

8.2.1 Coupling Arm and Pin Equations

To estimate the loads on the physical system, a free-body diagram was created to represent the tool and a moment equation was solved for the coupling arm force. Knowing the maximum coupling arm force allowed the relation between motor force output and the coupling arm force to be calculated for the various tool extensions. The system as a whole has only one degree of freedom resulting in numerous related geometric relationships. The configuration of the system and primary forces are shown in Figure 22. The force of the coupling arm against the bore-hole wall is F_w. The driving force for the coupling arm is created by the motor and projected through a motor drive rod shown as F_{rod}. Reaction forces are shown.

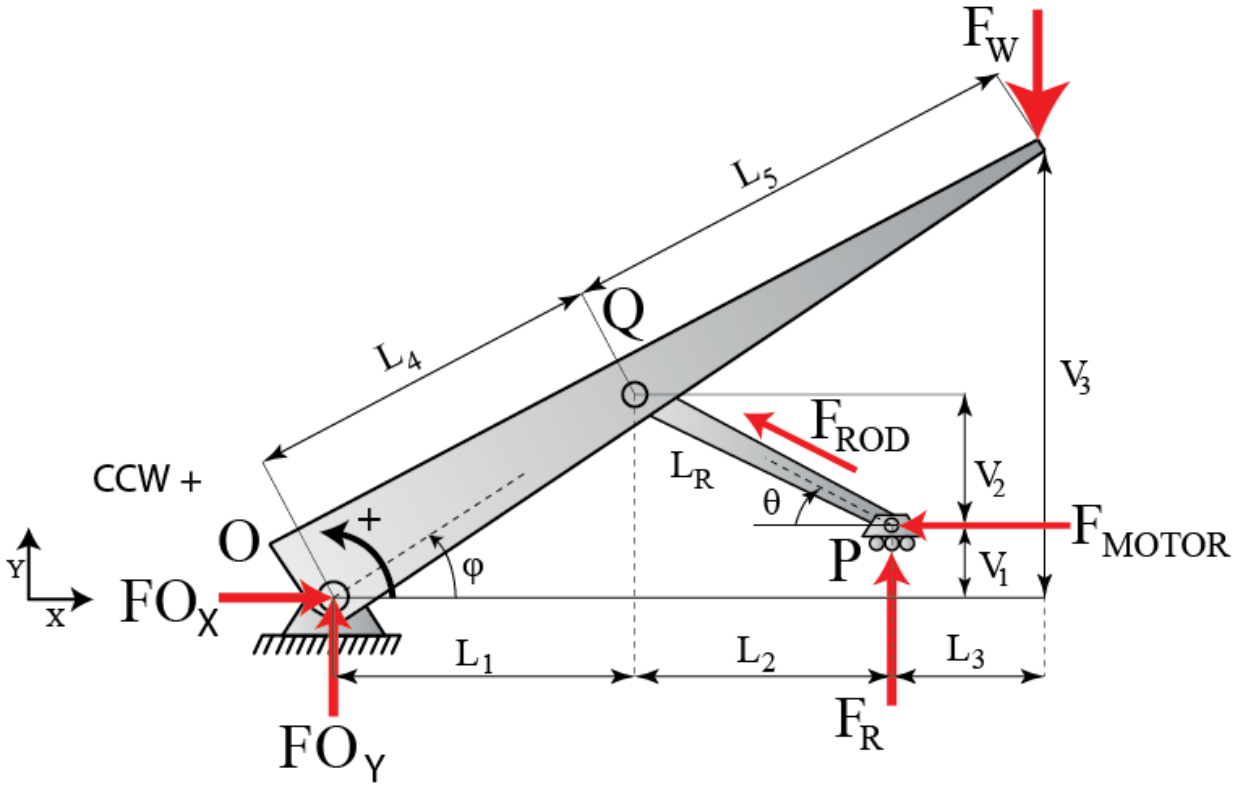

Figure 22: Coupling Arm Configuration

From the configuration of Figure 22, a free body diagram of the coupling arm was created as shown in Figure 23.

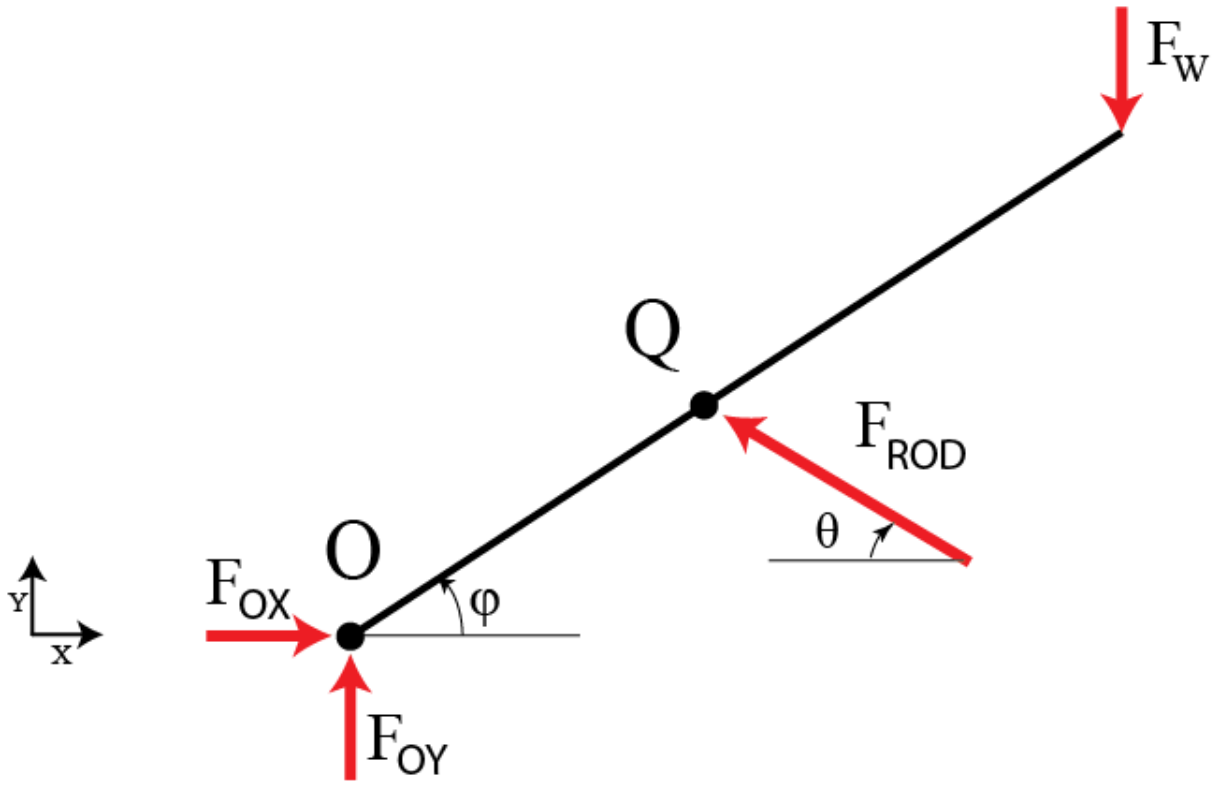

Figure 23: Coupling Arm Free Body Diagram

Once the free body diagram was drawn and all supporting geometric relations were characterized, the calculation of the moment at Point O was solved (Eq. [1]) as were the reaction forces at Point O (Eq. [2] and Eq. [3]).

$$Mo = -Fw(L1 + L2 + L3) + Frod\big(L1 * Sin(\theta) + (V1 + V2) * Cos(\theta)\big) \quad [1]$$

$$Rx = \Sigma Fx = FOx + L4 * \cos(\varphi) * Frod = 0 \quad [2]$$

$$Ry = \Sigma Fy = FOy - Fw + L4 * \sin(\varphi) * Frod = 0 \quad [3]$$

Equation (1) solves for F_{rod}. This value was divided into respective F_x and F_y component forces, allowing the relation of net motor force (no accounting of friction) to be directly related to the

force at the bore-hole wall (F_w). F_x and F_y are the reaction forces on a shear pin located at Point P, as shown in Figure 24.

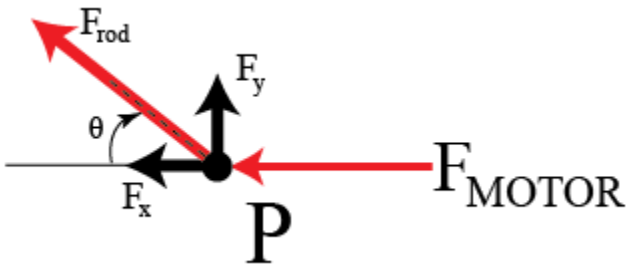

Figure 24: Pin Free Body Diagram

$$Fx = Frod * Cos(\theta) \quad [4]$$

$$Fy = Frod * Sin(\theta) \quad [5]$$

The shear pin is part of the tool design to allow retraction by force if the motor fails to function, in which case this pin would shear and free the tool for extraction up the hole. F_x and F_y were calculated to determine what forces the pin would have to withstand to allow the tool to produce the force required. The force equations were placed in a spreadsheet where numerous configurations could be evaluated based on tool geometry. The calculations were based on the position of the coupling arm, as this could be accurately measured. The forces measured and shown in Figure 20: *Coupling Arm Force* were evaluated in the spread sheet and estimates of frictional forces and maximum motor force were developed. Frictional forces were characterized as a function of F_w and θ (reference Figure 23). The supporting work for these calculations is found in Appendix F. Using the estimated frictional forces and the value of maximum motor force, estimates of forces at the wall were calculated. These are compared in Figure 25.

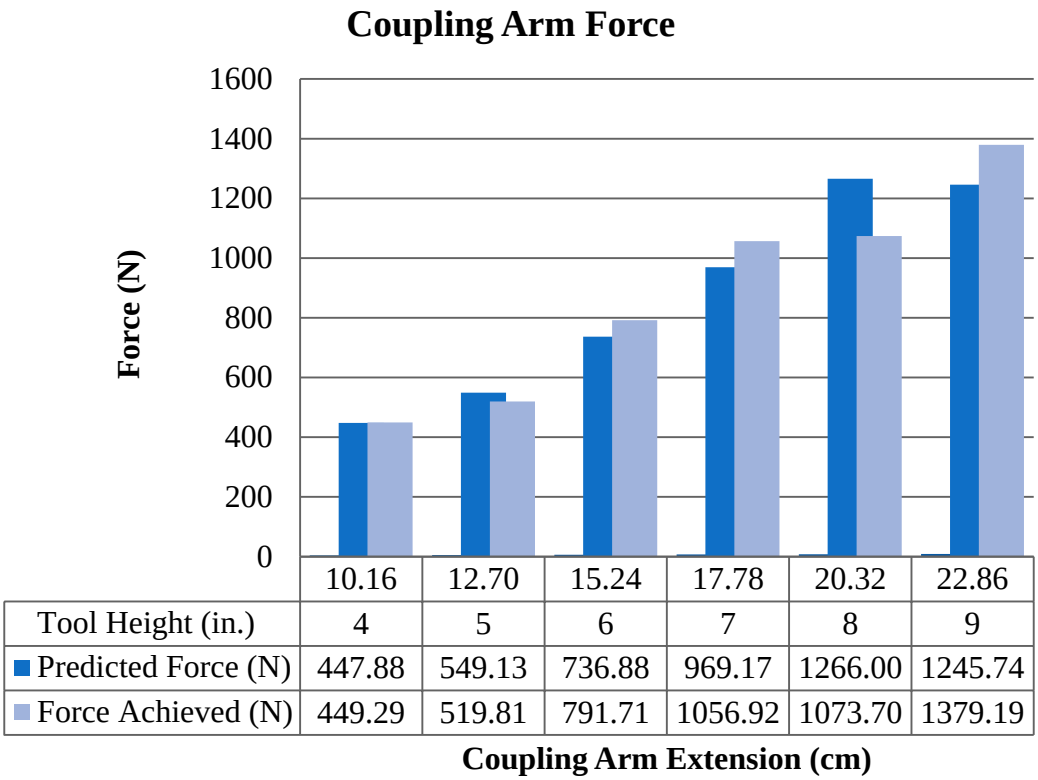

Tool Height (in.)	10.16	12.70	15.24	17.78	20.32	22.86
	4	5	6	7	8	9
Predicted Force (N)	447.88	549.13	736.88	969.17	1266.00	1245.74
Force Achieved (N)	449.29	519.81	791.71	1056.92	1073.70	1379.19

Figure 25: Coupling Arm Force Calculated vs. Measured

The predicted force values were all trending relatively closely to the measured values but due to equation simplification, (not including all mechanical losses), the predicted values were slightly off as shown in Figure 25. Observing the data, the measured force value at 20.32 cm (8in.) seems to be incorrect which resulted in a larger error of prediction at that extension. At the lower coupling arm extensions, the majority of the motor force would be applied in an axial direction while only a fraction of the force would be applied radially out. This resulted in a low coupling arm force of 449 N (101 lbf.) at the 10.16 cm (4 in) contact point with the bore-hole wall.

The motor force was inadequate to achieve the needed values of F_w at all extensions, but this could be addressed by a new motor gear box that would have higher torque and create a higher axial force.

8.2.2 Motor Gear Box Calculation

The seismic tool was required to produce an equivalent of 1,779 N (400 lbf.) at the 10.62 cm (4.18 in.) extension (at the minimum extension level). Based on the relation of torque-to-force at the 10.62 cm (4.18 in.) bore-hole wall, the required gear ratio could be solved for. Using interpolation, a relationship was established between the maximum force the tool could produce at the bore-hole wall, to the torque output of the motor, and subsequently the required gear reduction ratio. Taking three known values, one unknown was solved for at a time. The steps taken to solve for the ratios shown in Table 6 are in Appendix G.

Table 6: Gear Box Calculation

Required Motor Torque			
RATIO	**MAX TORQUE (oz-in.)**	**MAX TORQUE (Nm)**	**MAX Fw (N)**
524.60	366.00	2.58	448.73
639.90	445.00	3.14	545.59
780.60	544.00	3.84	666.97
2077.62	**1449.50**	**10.24**	**1777.15**

To verify gear reduction ratio assumptions were correct, calculated values were compared to those provided on the motor specifications sheet. Based on the calculations, the motor would require a gear reduction ratio of about 2078 to 1. The motor manufacturer, Globe Motors, was contacted to obtain data about their motors and gearbox options. The resulting motor gear box chosen has a 3,382 to 1 gear reduction ratio with the same motor mount. This replacement motor meets and exceeds the required motor ratio as shown in orange in Table 6 and could be directly swapped with the exiting motor.

8.2.3 Electrical Current Sensor Calculation

From the initial electro-mechanical test, the current sensor provided very little useful data because the current seen by the sensor exceeded the measurable limit. Globe Motors estimated the maximum ampere rating for the motor to be 1.78 A as shown in Appendix H. A slight modification to the current sensor was made to reduce the gain so the current seen would result

in meaningful data, which followed the same steps in Section 7.3.1 *Procedure for Testing Current Sensing*. Additionally, the high temperature operational amplifier had to be replaced because it had been damaged by an electrical short. This error could have resulted from not properly grounding the circuit so precautions will be taken to ensure components are grounded.

8.3 Final Electro-Mechanical System Test

Based on the calculations described in Section 8.2.3, new resistors were installed in the operational amplifier circuit while keeping the original shunt resistor. Since the motor was unable to produce the required force on the coupling arm, the system was again tested to motor stall. Comparing the initial to final force values of the electro-mechanical systems test would ensure repeatability and the new data would yield the appropriate current-to-force relationship. The rationale for this confirmatory test was based on the premise that the existing motor with a new gear box could provide adequate power for field applications. The new gearbox would generate more torque and greater force to the shear pin that drives extension of the coupling arm. Following the same test procedure from Section 8.1.2 *Procedure for Electro-Mechanical System Test*, the new torque sensor (modified with the new op amp) results were found to correlate as predicted to the coupling arm force.

8.3.1 Results

Testing was conducted at coupling arm extensions of 10.16 cm (4 in.), 12.70 cm (5 in.), 15.24 cm (6 in.), 17.78 cm (7 in.), 20.32 cm (8 in.), and 22.86 cm (9 in.) to simulate conditions in bore-holes of these same diameters. The data established the relationship between motor electrical current and coupling arm force as a function of bore-hole diameter. At each extension, the motor was supplied 24 volts and ran until motor stall resulting in varying forces at the load cell.

Figure 26 shows one example of the force seen by the load cell as a function of time. While conducting the test, power was supplied until the motor stalled. At the point of stall, power was removed for approximately three seconds, and then reapplied to help determine the force lost when the system was allowed relax (absorb mechanical compliance based on construction tolerances, that is, slack).

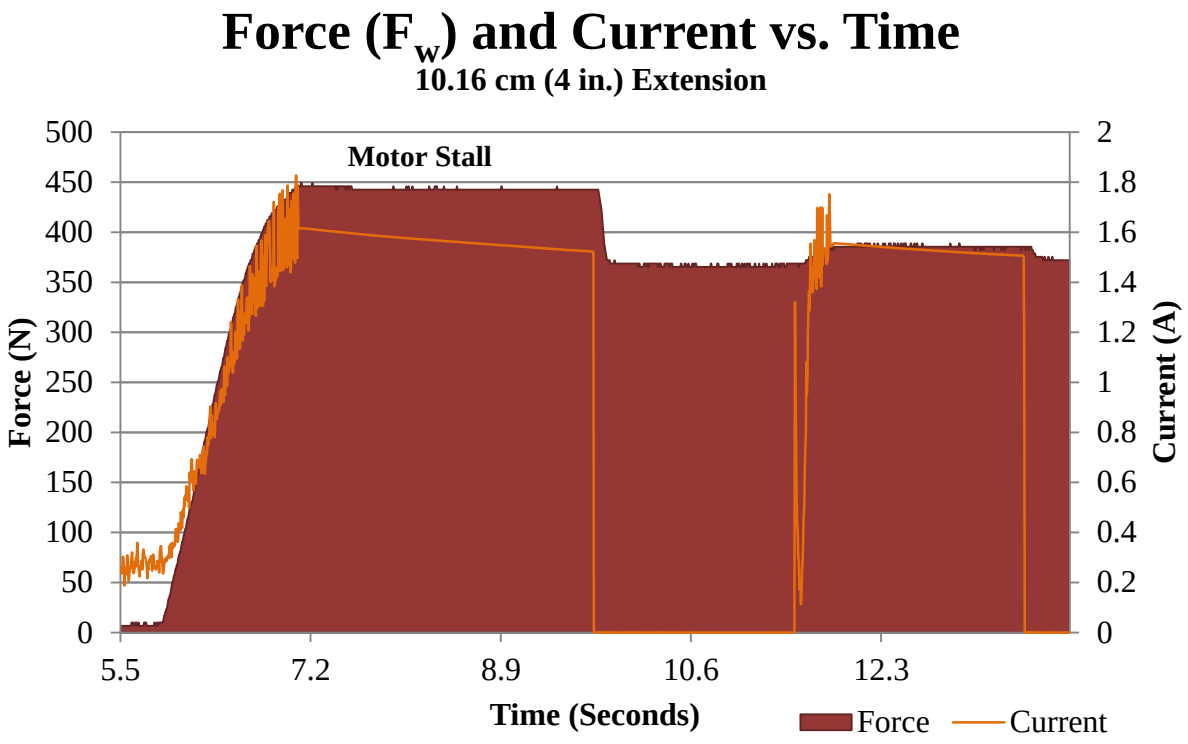

Figure 26: Force (F_w) and Current vs. Time at 10.16 cm (4 in.) extension

Based on Figure 26, the maximum force (F_w) produced by the motor, at motor stall, was about 450 N but dropped to 350 N when power was removed shown in red. Additionally, the current was recorded during testing. These values were used to characterize the motor performance at the 10.16 cm (4 in.) coupling arm extension. The current steadily increased as a function of force seen at the coupling arm but there was noise in the signal. Each coupling arm extension has a different force (F_w) -to-current ratio. Figures 26 through 30 show comparable data for the remaining coupling arm extensions.

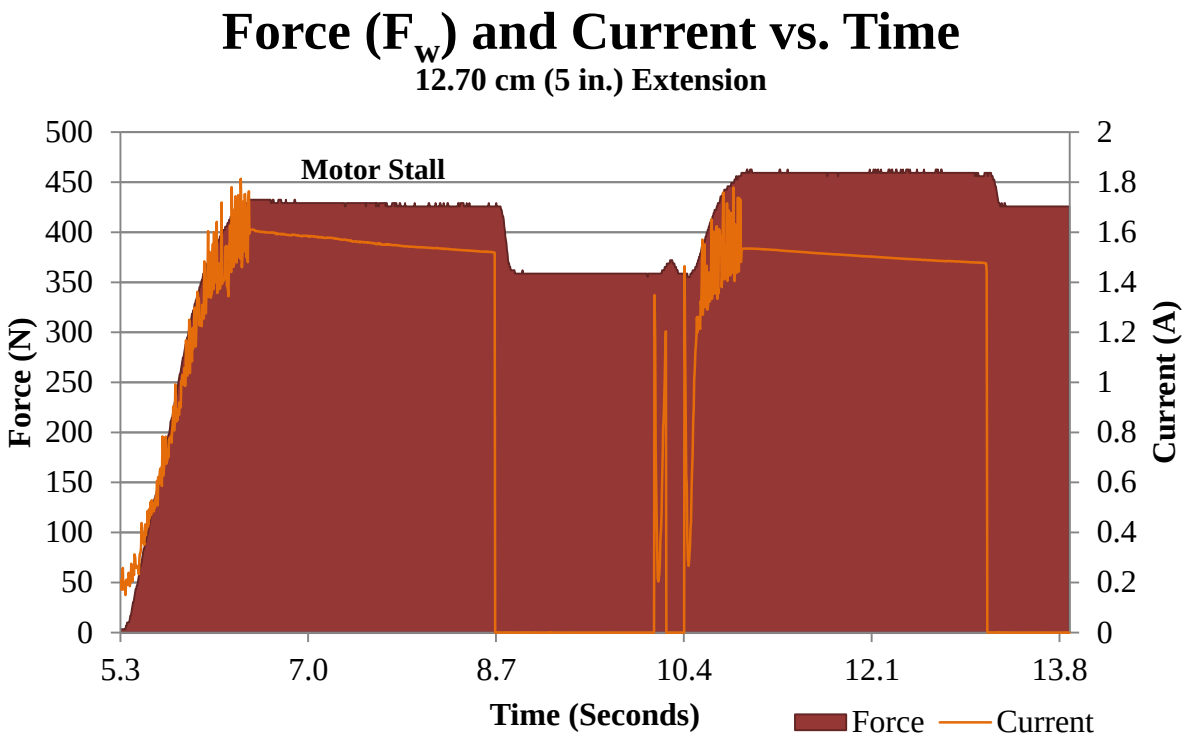

Figure 27: Force (F_w) and Current vs. Time at 12.70 cm (5 in.) extension

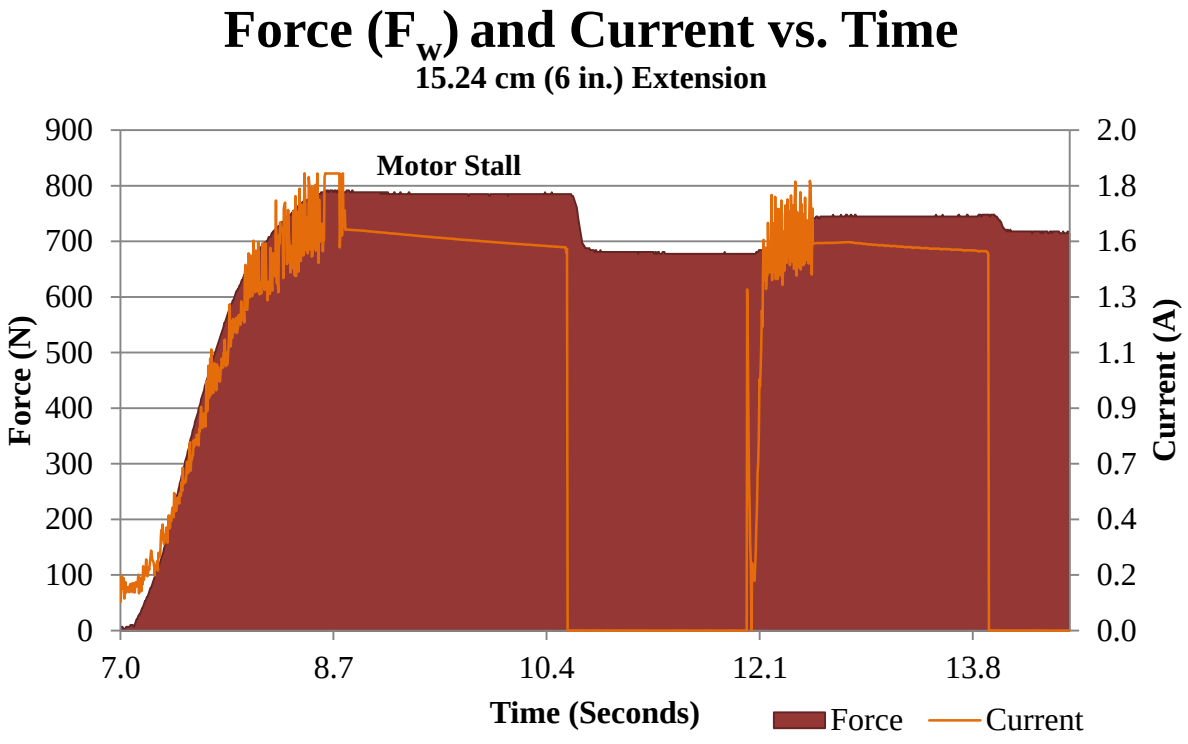

Figure 28: Force (F_w) and Current vs. Time at 15.24 cm (6 in.) extension

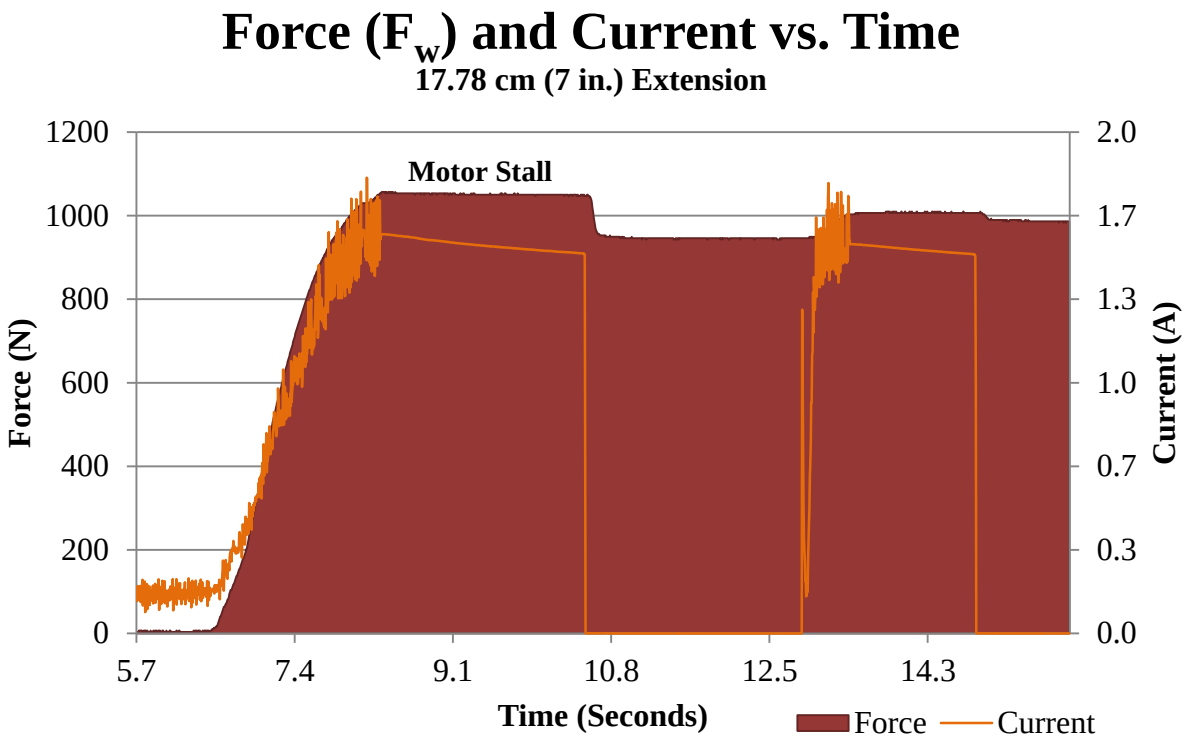

Figure 29: Force (F_w) and Current vs. Time at 17.78 cm (7 in.) extension

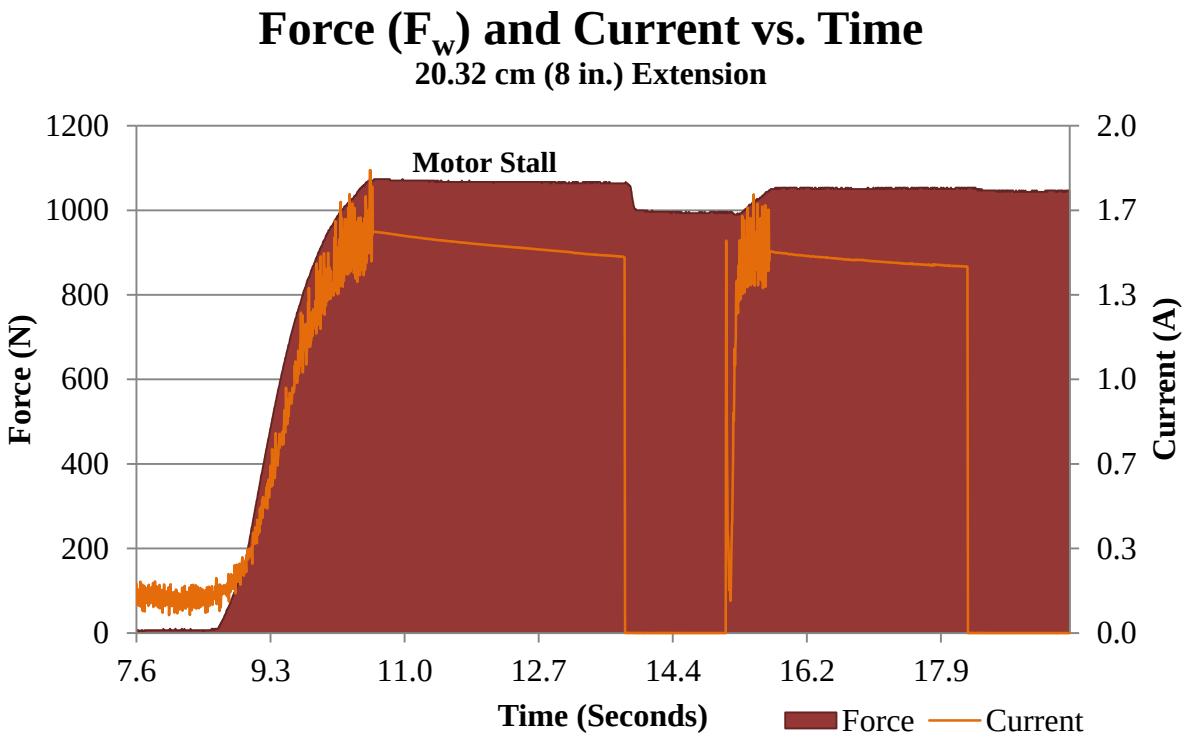

Figure 30: Force (F_w) and Current vs. Time at 20.32 cm (8 in.) extension

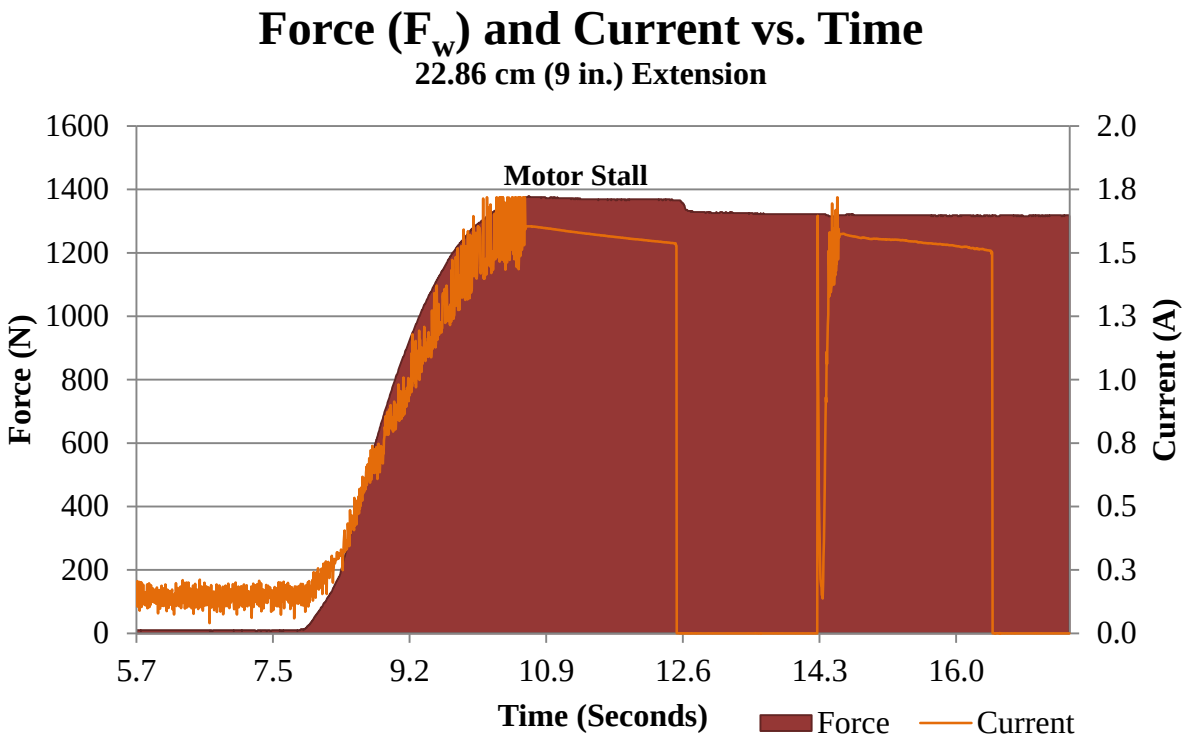

Figure 31: Force (F_w) and Current vs. Time at 22.86 cm (9 in.) extension

Evaluation of these data show that as the coupling arm extension increased, the amount the system relaxed decreased which resulted in a greater sustained coupling force at the bore-hole wall. This was further supported by the calculations done in Section 8.2 *Intermediate Design Calculations Based on Initial Tests* where the axial load decreased as coupling arm extension increased. Furthermore, when current was supplied after the initial coupling of the tool, a large spike of current was often seen. A software solution will be required to address these uncontrolled electrical spikes to ensure that the seismic tool is secured with the correct force.

8.4 Electro-Mechanical System Test Summary

The motor torque sensor worked as needed. At each of the different coupling arm extensions, the current sensor measured values which correlated with the force applied by the coupling arm. Once these electrical current values were established and categorized based upon bore-hole diameter, they were input as threshold limits into the controller unit. The values were specifically picked to ensure a consistent force would result between the coupling arm and bore-hole wall when the motor is actuated. With the controller programmed, threshold values can be selected by a seismic test tool operator based upon the supplied bore-hole diameter where the

measurements are being made. With the electro-mechanical system testing completed, the process of integrating the micro-processor into the rest of the system could begin.

Chapter 9. PHASE 3: INTEGRATED SOFTWARE-ELECTRO-MECHANICAL SYSTEM TESTING

The Phase 3 testing objective was to produce a closed-loop solution allowing the tool to extend until the coupling arm reaches the predetermined 1,779 N (400 lbf.) with the bore-hole wall. Because the motor gear ratio was too high to achieve the required force, the maximum force achievable was used as the basis for system testing. When the proper gearbox is obtained electro-mechanical system tests will have to be repeated to obtain the correct current-to-force relationship values. Using the information provided by Section 8.3 *Final Electro-Mechanical System Test*, the controller program was modified to operate the coupling arm.

9.1 Software Controller Testing

Throughout component testing, code was being developed for controlling the system. Using a reprogrammable FPGA, numerous programming iterations were conducted to achieve the desired results for tool process control. The FPGA would read in the current sensor data and if the force was below the desired threshold, the motor would continue to run until the required force was met as indicated by the voltage across the shunt resistor. The code eventually used followed the flow diagram shown in Section 5.3, Figure 8: *Current Sensor Code Sequence*. The code executes based on a sample rate which was programmed into the FPGA. At the sampling rate set by the operator, the controller would send a signal to obtain the motor torque which was the parameter used in the feedback loop to control coupling arm force on the bore-hole wall.

9.1.1 Equipment

The equipment used to conduct these system tests was categorized as either physical supporting equipment or electrical diagnostic equipment. All testing was conducted in a laboratory setting.

9.1.1.1 Physical Supporting Test Equipment

This testing employed the items listed in Table 7 and the test setup is shown in Figure 32.

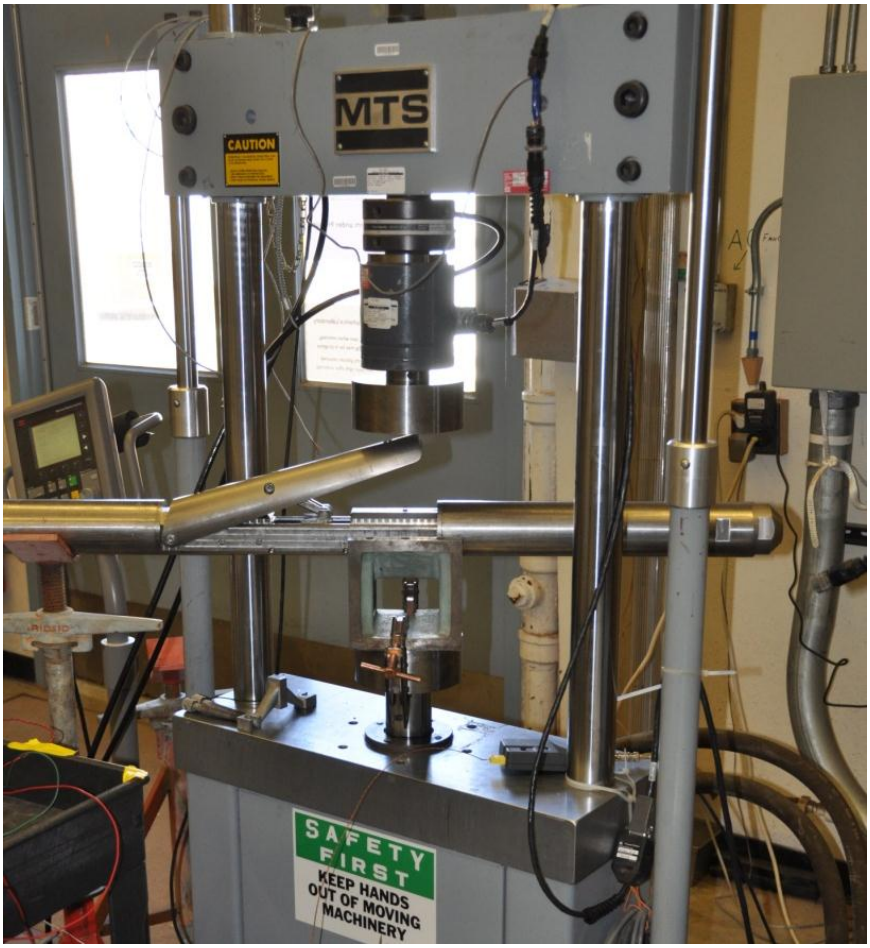

Figure 32: Integrated System Physical Support Equipment

Table 7: Integrated System Physical Support Equipment

Item Number	Item Name	Use
1	BK Precision 1761 DC Power Supply	Triple output power supply. 24V to motor, 7V to FPGA board, 5V to current sensor.
2	Globe Motor 5A4445	DC motor.
3	One-Piece Rigid Coupling	Rigid coupling used to connect motor to shaft for motor testing.
4	Rigid ™ Support Frame	Provide support to complete tool when tested under load cell.
5	Seismic tool	Seismic tool body which houses the motor and coupling arm mechanics.

9.1.1.2 Electrical Diagnostic Test Equipment

Table 8 lists the electrical diagnostic equipment used in the system level tests. Figure 33 shows the FPGA connected to a MOSFET (a high power switch). When high signal is sent to the MOSFET, 24 volts of power is supplied to a low temperature dc motor.

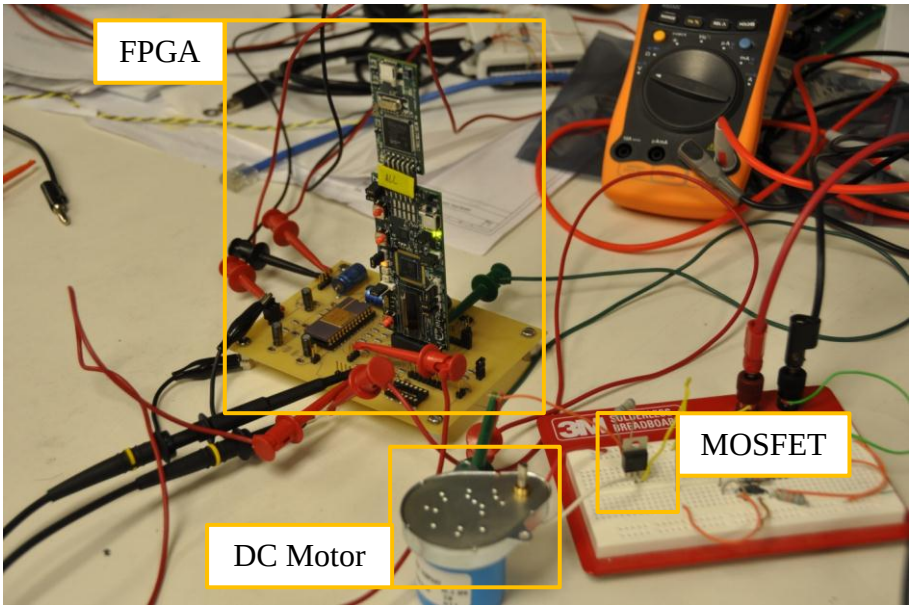

Figure 33: Integrated System Diagnostic Test Equipment

Table 8: Integrated System Diagnostic Test Equipment

Item Number	Item Name	Description and Use
1	K-type Thermocouple	Thermocouple used with digital thermometer.
2	MTS Load Cell	Obtain force produced by coupling arm.
3	Data Acquisition System	Captured load cell data, voltage reading from current sensor, and motor temperature.
4	HTOP01	High Temperature op-amp used to build production current sensor.
5	Resistors	Supporting circuitry for building current sensor.
6	Windows Based Computer	Required to run software to program FPGA.
7	Libero IDE	Software Used to program FPGA.
8	FPGA	Reprogrammable processors.
9	MOSFET	A high voltage switch that opens when supplied a low voltage.
10	24 V DC Motor	A low temperature motor used to test FPGA code.
11	USB Cables	Used to connect FPGA to computer.

9.1.2 Software Controlling Testing Procedure

Once the tool controlling software was compiled, the controller board was tested in the lab to verify that the software worked. With the use of an oscilloscope, two channels were used to verify the functionality of the code before connecting a motor to the circuit by connecting the scope to the output pin controllers. Channel 1 monitored the sampling frequency of 20 kHz. Channel 2 monitored the signal for the motor to turn on based on a threshold value programmed onto the board. While in operation, the FPGA would look for a voltage provided by a manually controlled voltage source at the sampling frequency. This was facilitated by the code operating on a pulse out signal matching the sampling frequency. Once the voltage reached a value greater than a 2.5 volt threshold, the FPGA would send a high signal (3.3 volts) to a MOSFET controller switch, allowing 24 volts to be applied to the motor. Inversely, once the voltage decreased below the 2.5 volts, the motor would turn off. The manually supplied voltage to the FPGA would be later replaced by the voltage out provided by the motor current sensor.

9.1.3 Results

The 20 kHz sample frequency was synchronized to a pulse out command, executing the process of reading the motor current sensor value. Comparing the current sensor value to the threshold allowed the controller to send either a high or low signal to the motor. If the signal was high, the motor would turn on and if the signal is low, the motor would turn off. The plots below (Figure 34 through Figure 37) confirm the 20 kHz sampling frequency (yellow) and the motor control (blue).

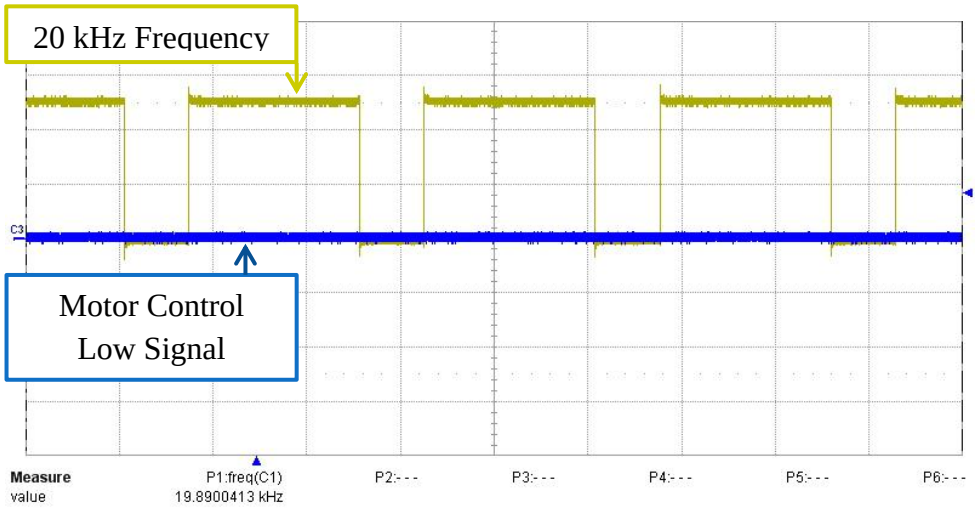

Figure 34: Oscilloscope Verification Low Motor Signal

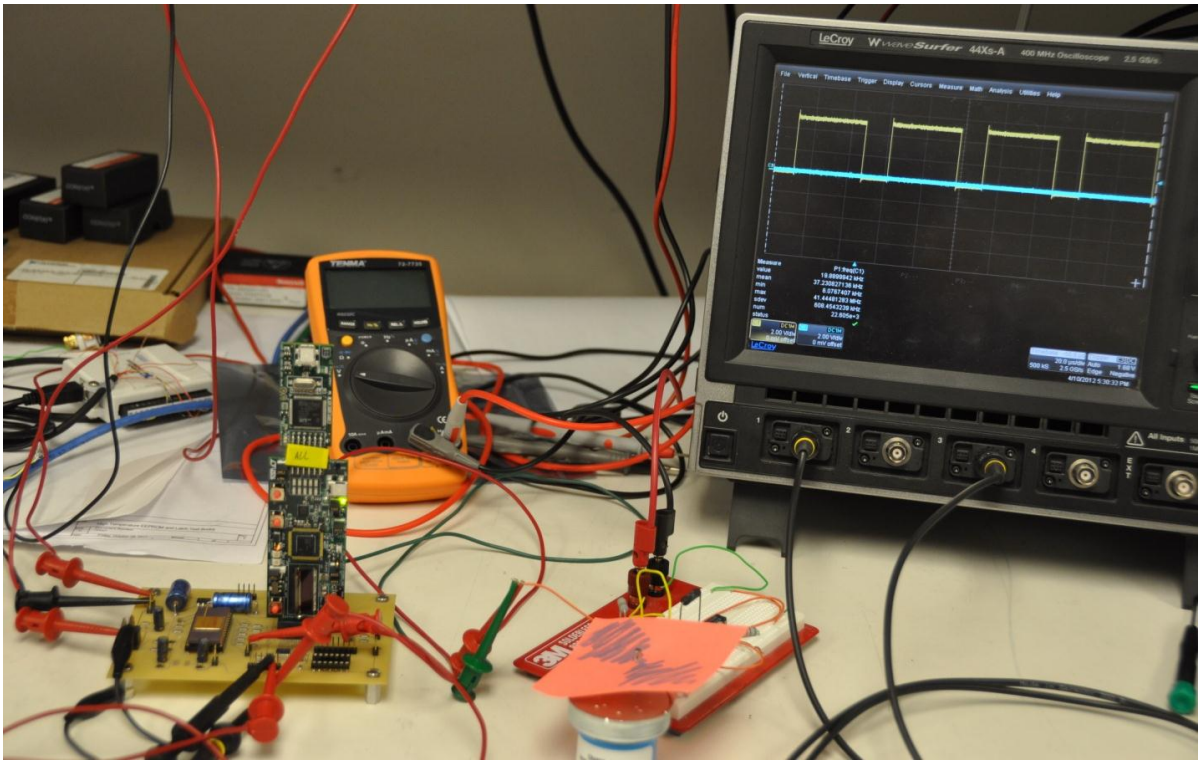

Figure 35: Oscilloscope Verification Set-up (Low)

Once the input signal was greater than 2.5 volts, the motor output signal would go high. When the MOSFET was supplied 2.5 volts, it would allow the 24 volt source to complete the circuit and run a motor.

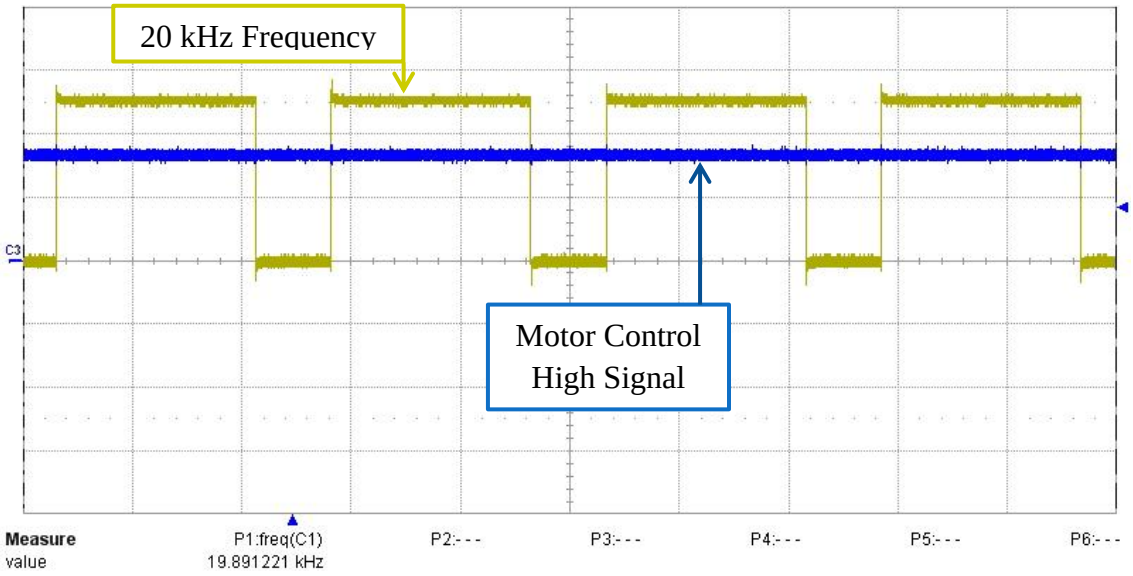

Figure 36: Oscilloscope Verification High Motor Signal

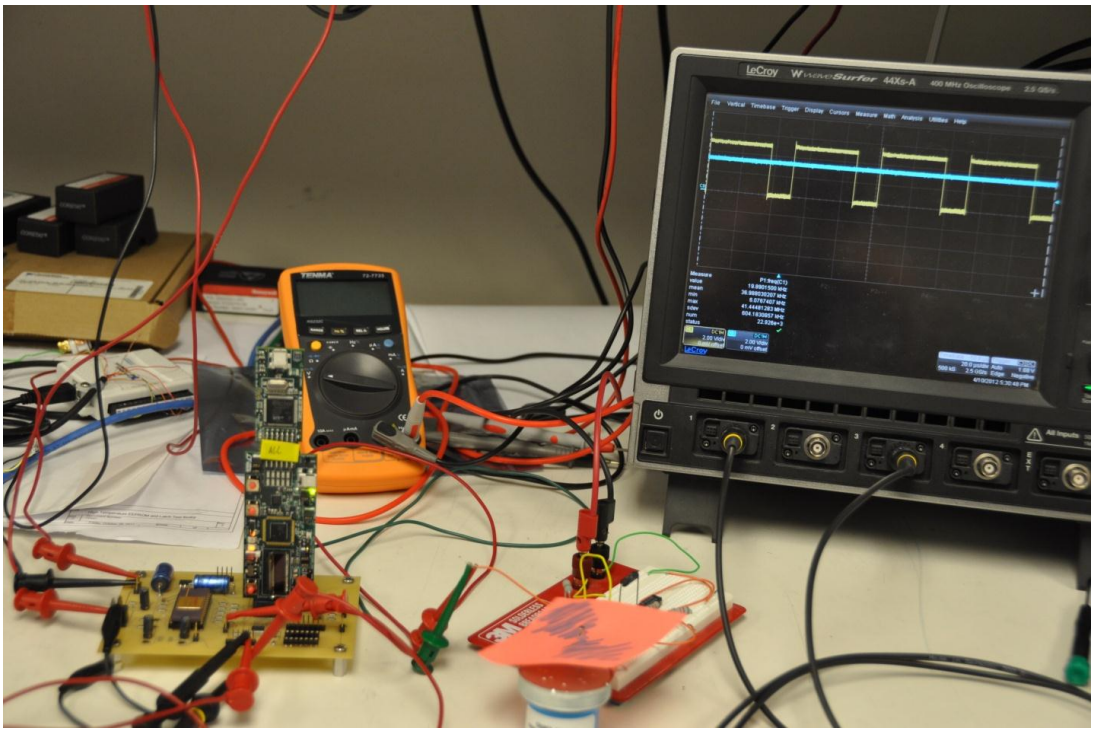

Figure 37: Oscilloscope Verification Set-up (High)

9.1.4 Software Performance/ Conclusion

The code worked as expected and a few modifications were made for the system test. Modifying the threshold value would change the point at which the coupling arm would stop advancing. Since the torque and force produced by the motor was less than required for application in the field, modified threshold values were required to work within the operational range of the motor. From the information provided in Section 8.3 *Final Electro-Mechanical System Test*, the voltage out relationship with the load produced by the coupling arm was known. Each of these threshold values would be correlated with the extension of the coupling arm. The final iteration of the code requests the size of the bore-hole to be entered by the operator and the correct threshold value will be automatically supplied to the tool. Once fitted with an appropriate gear box, when the coupling arm reaches the required 1,779 N (400 lbf.), the motor will shut off and the tool would be held secure allowing micro-seismic data to be collected.

9.2 System Testing and Evaluation

Once component tests were completed, the complete system test could begin. Figure 38 shows the complete testing setup.

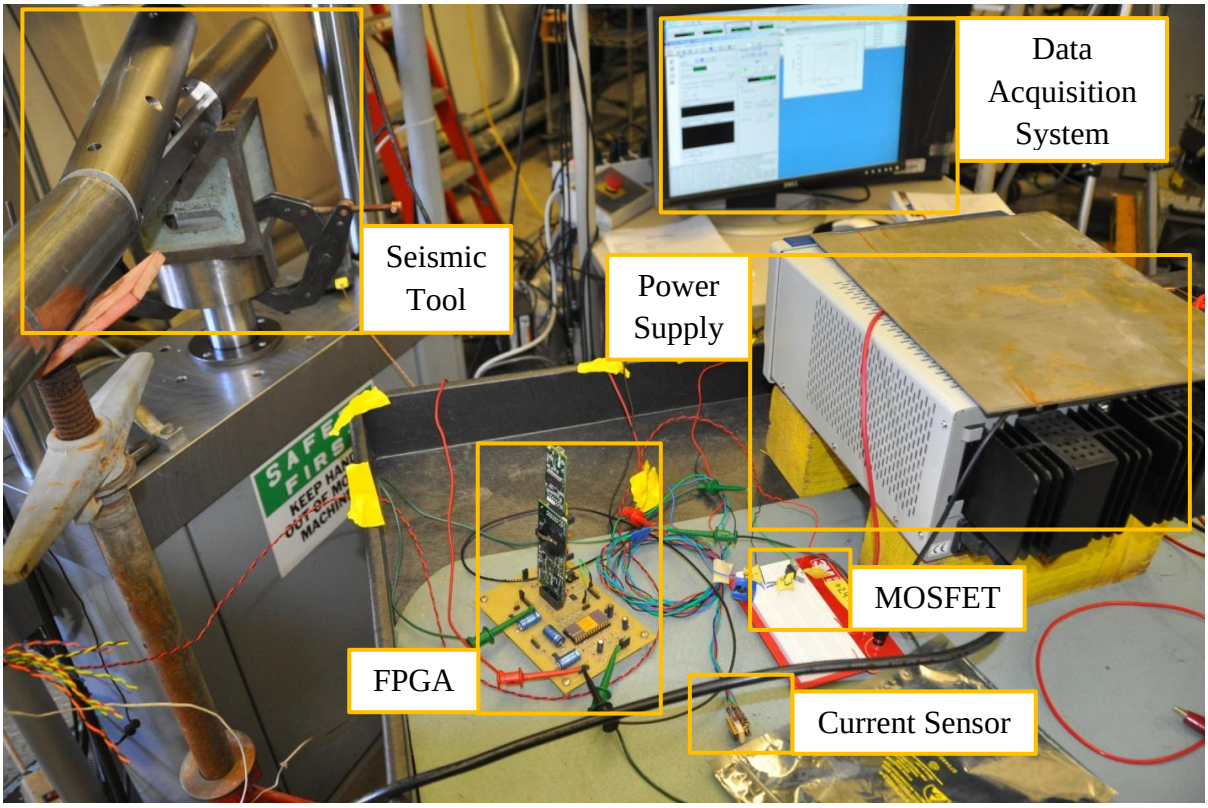

Figure 38: Final System Testing

9.2.1 Procedure for System Testing

To begin the system test, the completed tool was taken to the rock mechanics laboratory and placed under a load cell with the tip of the coupling arm directly under the load cell sensor. When the tool was supplied 24 volts, the coupling arm would extend radially until contact with the load cell was achieved. While in motion, the FPGA would read the motor current sensor. If the current sensor value was greater than the programmed threshold value, the motor would stop because sufficient torque was being applied to achieve the desired force. To ensure the coupling arm successfully reached and maintained the desired force, the load cell data was monitored and recorded.

A threshold value was established at 1.08A for the 17.78 cm (7 in.), 20.32 cm (8 in.), and 22.86 cm (9 in.) extension values. Figures 28 through 30 were evaluated to determine what the expected F_w would be. The system was tested to confirm that the motor and resulting forces were controlled as desired. The detailed testing procedure is in Appendix I.

9.2.2 Results

The force levels generated for this test were achieved by turning the motor on while the current sensed was less than the threshold value. At each of the coupling arm extensions, the threshold value was set to stop the motor at a predetermined location which corresponded to the appropriate coupling force. The threshold was set at 1.08 A for all tests to quickly confirm tool performance. The desired force is the force achieved based on data collected in Section 8.3 *Final Electro-Mechanical System Test*. The point at which the current passed the threshold value is shown in Figure 39 through Figure 41 and the corresponding force was recorded for comparison to the system test results.

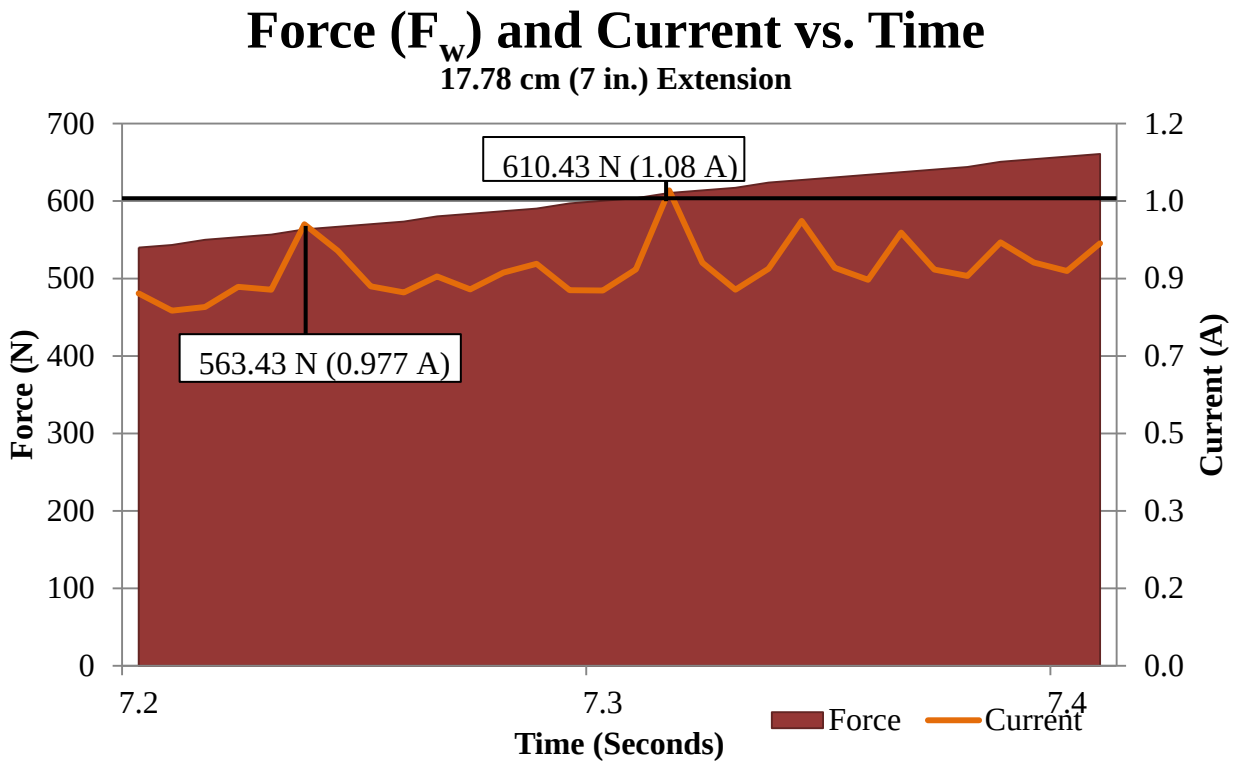

Figure 39: Force (F_w) and Current vs. Time 17.78 cm (7 in.) Extension

Figure 39 shows the point at which the current exceeded the threshold value. The force associated with the threshold current value was 610.43 N (137.23 lbf.) at the 17.78 cm extension. Due to noise in the current sensor, a current spike was seen at 563.43 N (126.66 lbf.), which could be close enough to the threshold value to cause a false force reading resulting in the motor stopping before the desired force was achieved.

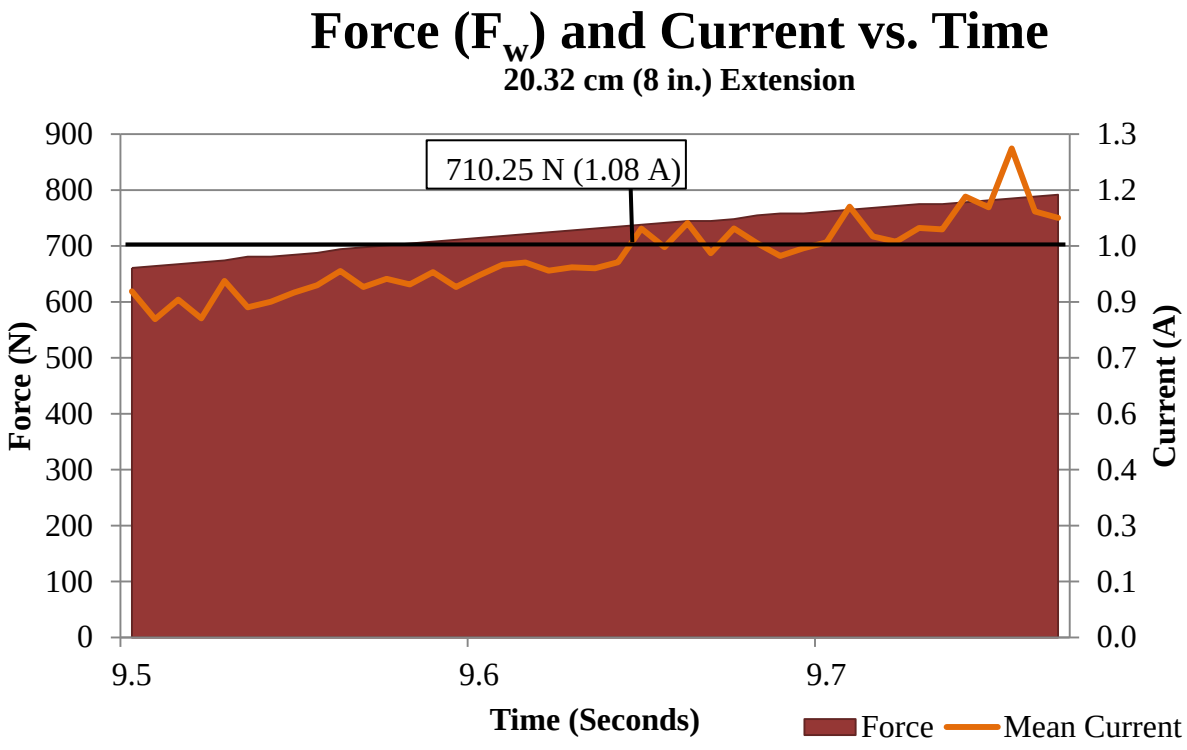

Figure 40: Force (F_w) and Current vs. Time 20.32 cm (8 in.) Extension

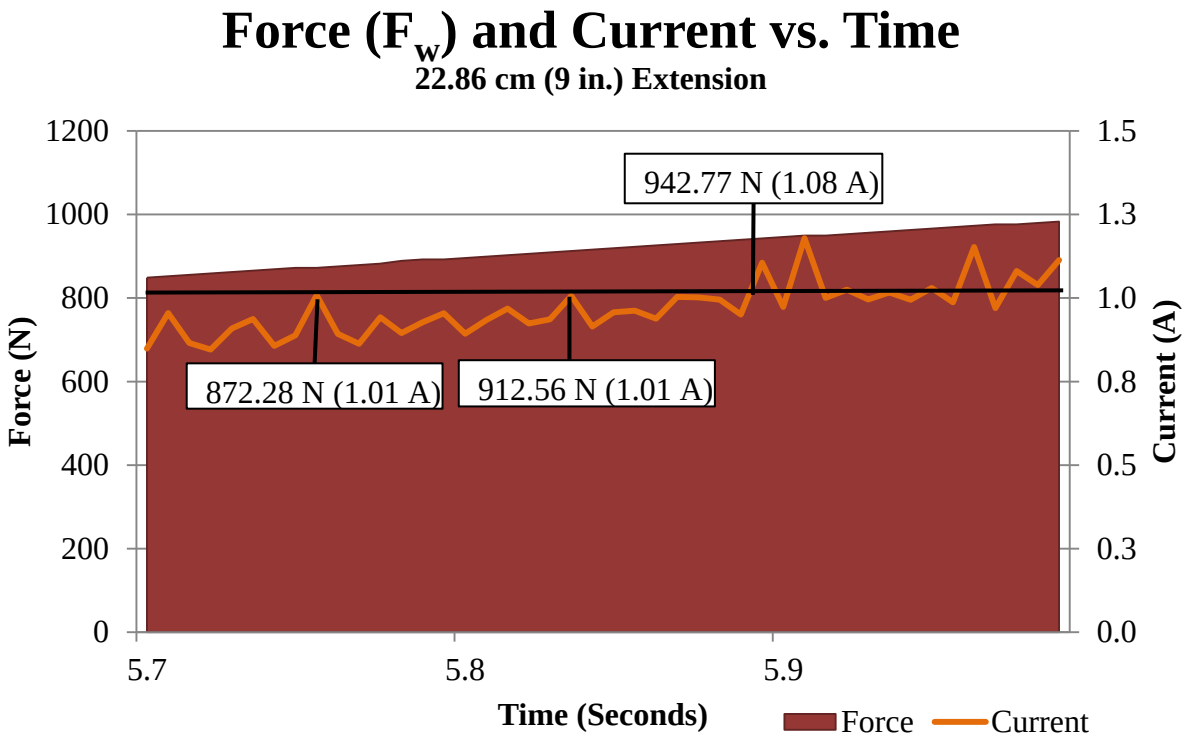

Figure 41: Force (F_w) and Current vs. Time 22.86 cm (9 in.) Extension

With the correct threshold values saved, the integrated controller testing could begin. The testing results are graphically summarized in Figure 42 to Figure 44.

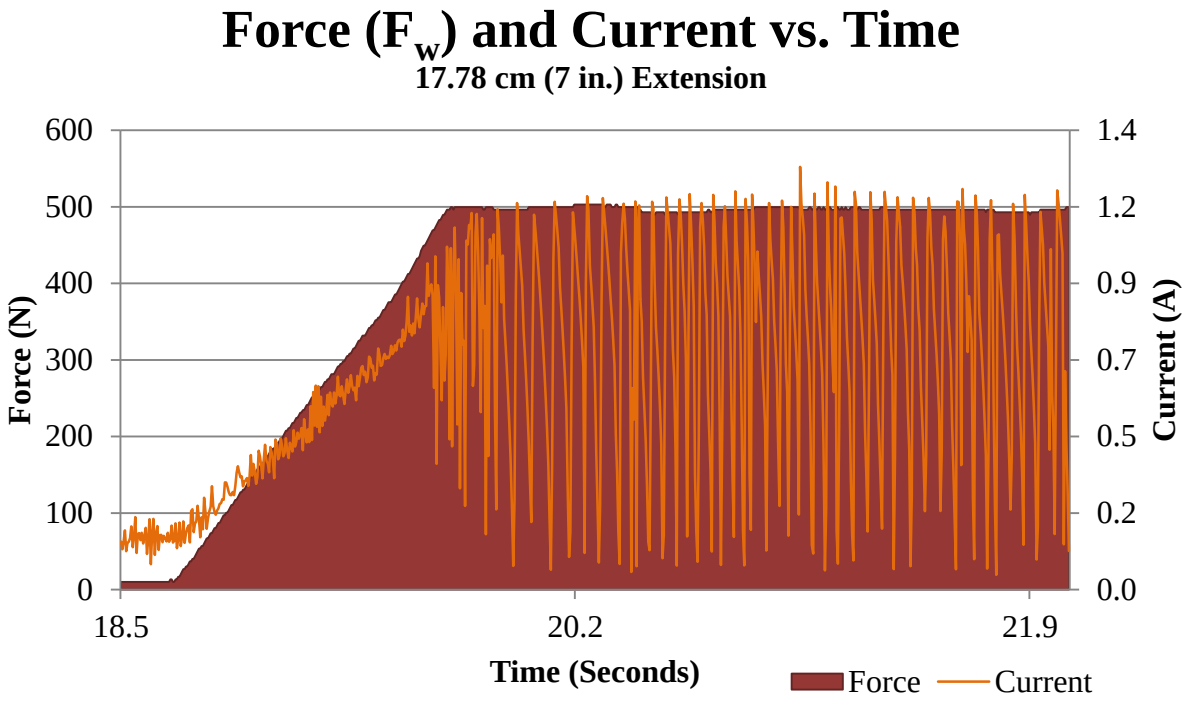

Figure 42: Controlled Coupling Arm Extension Force (F_w) at 17.78 cm (7 in.)

The current shown in Figure 42 (orange line) shows heavy oscillations because the controller compared the current value to the threshold value continuously. As soon as the desired current was detected, current was removed from the motor which subsequently triggered the controller because the current threshold value was not met, which activated the motor and the cycle would repeat. This process continued for the duration of the test. The force is held constant over the test duration. Elimination of the motor signal cycling can be easily achieved by programming the controller to stop the motor once initial conditions have been met.

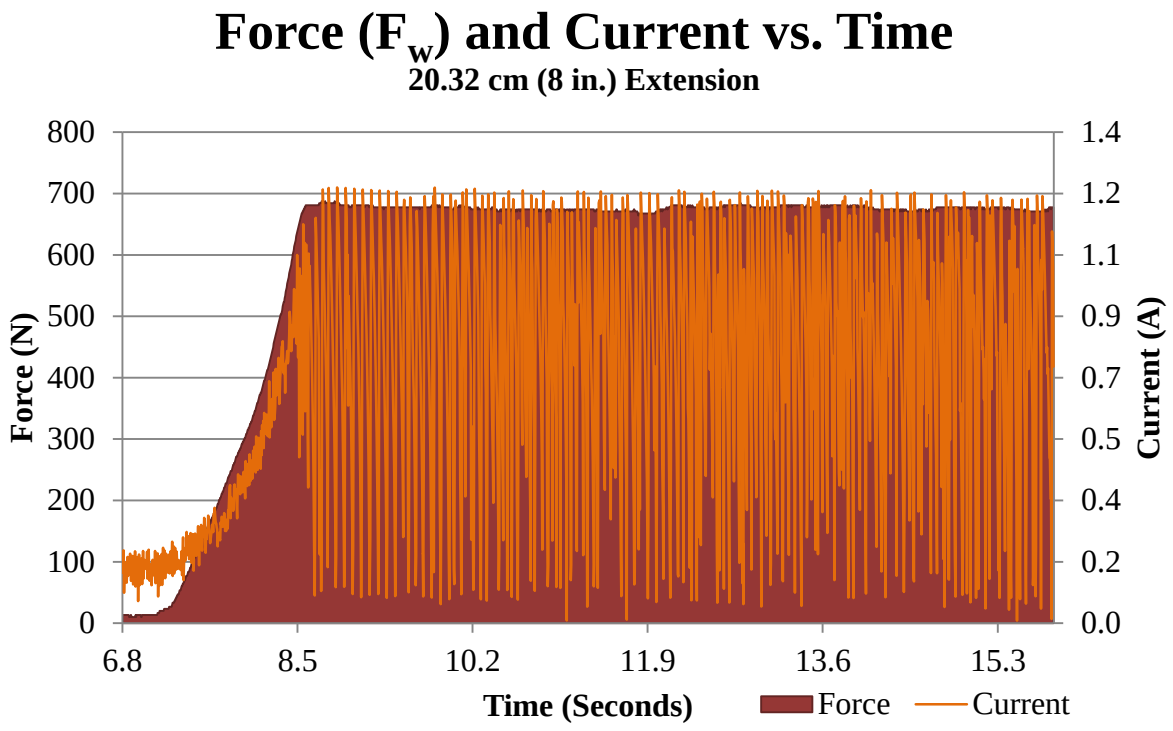

Figure 43: Controlled Coupling Arm Extension Force (F_w) at 20.32 cm (8 in.)

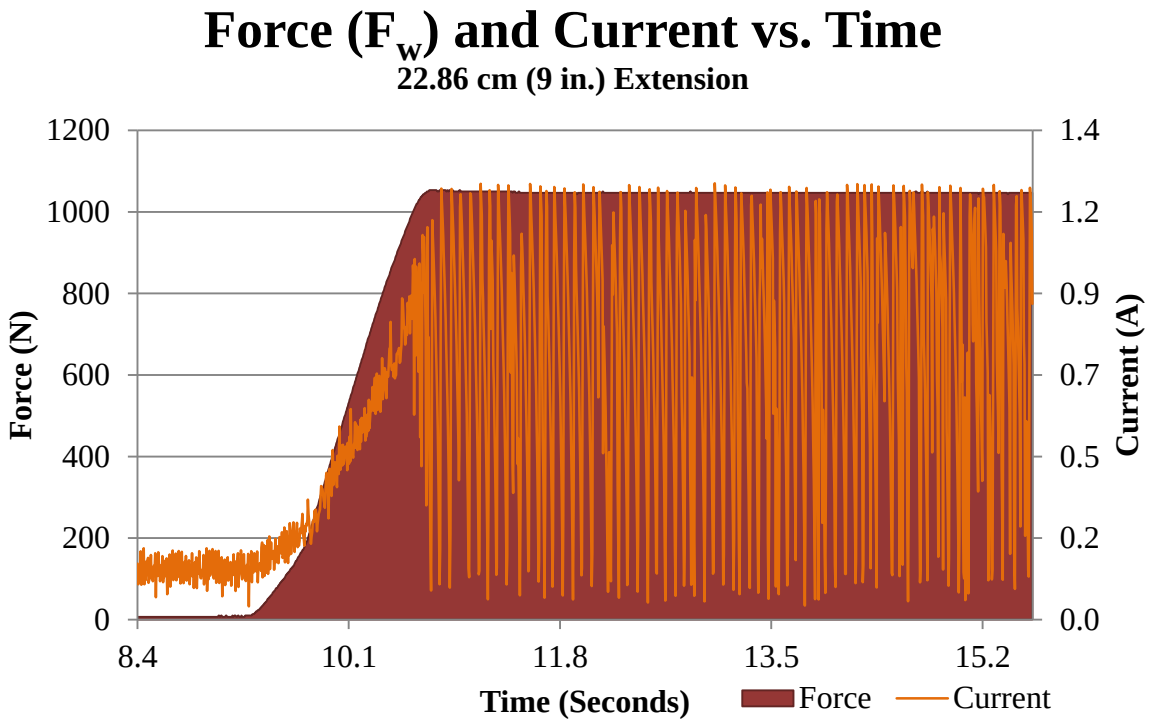

Figure 44: Controlled Coupling Arm Extension Force (F_w) at 22.86 (9 in.)

9.3 System Results Summary

Once testing was completed, the desired force values were compared to the obtained controlled force values shown in Table 9.

Table 9: Current Sensor Performance

Current Sensor Performance								
Extension (cm)	**Desired Force (N)**	**Controlled Force (N)**	**Difference (N)**	**Extension (in.)**	**Desired Force (lfb.)**	**Controlled Force (lbf.)**	**Difference (lbf.)**	**% Error**
18.24	610	503	-107	7.18	137	113	-24	**-17.54**
20.78	710	677	-33	8.18	160	152	-7	**-4.65**
23.32	942	1043	101	9.18	212	234	23	**10.72**

Test results confirmed the FPGA code worked but there were errors in accuracy. As the coupling arm extended, the accuracy was irregular shown in Table 9 (see the % error data). At the 18.24 cm (7.18 in.) extension, there is a difference of -107 N (24 lbf.) between the desired force and that applied by the system, a difference of -17.54%. At the operator interface level, modifications will have to be made to modify the threshold value as needed to meet field conditions by selecting the bore-hole diameter.

Chapter 10. DISCUSSION AND CONCLUSION

10.1 Discussion

10.1.1 System Performance Observations

System performance results confirmed that when the bore-hole diameter is selected, the coupling arm extends and could reach the appropriate force, within 100 N (25 lbf.). Three design modifications could aid in sensor accuracy. First, obtaining an accurate threshold value depends on the accuracy at which the coupling arm extension can be measured. At each extension, the force-to-current relationship changes, thus affecting the threshold value. During testing a ruler was used to measure the distance between the tool housing and the load cell. To increase the accuracy of this measurement, a sensor should be mounted to the surface of the tool to record the distance to the load cell platen. The data collected from the distance sensor could then be

recorded by the data acquisition system during testing. Second, to increase accuracy of the sensor, further code modifications need to be made to average the current sensor values because of the variations seen in Figure 45 to Figure 47. Averaging ten current input values (labeled as mean current) would result in less noise seen by the FPGA microprocessor. This would eliminate the possibility of sensing a faulty current reading. A comparison of current sensor data against mean current sensor data is shown below.

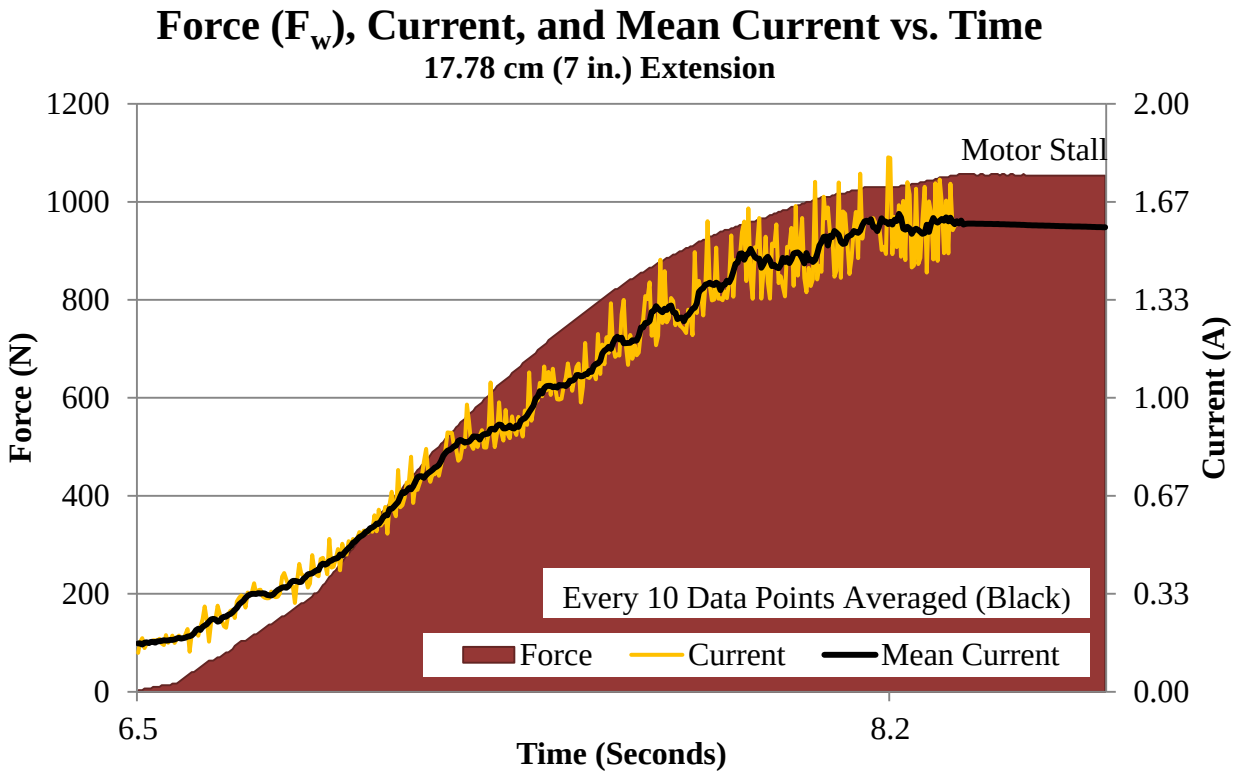

Figure 45: Force (F_w), Current, and Mean Current vs. Time at 17.78 cm (7 in.) Extension

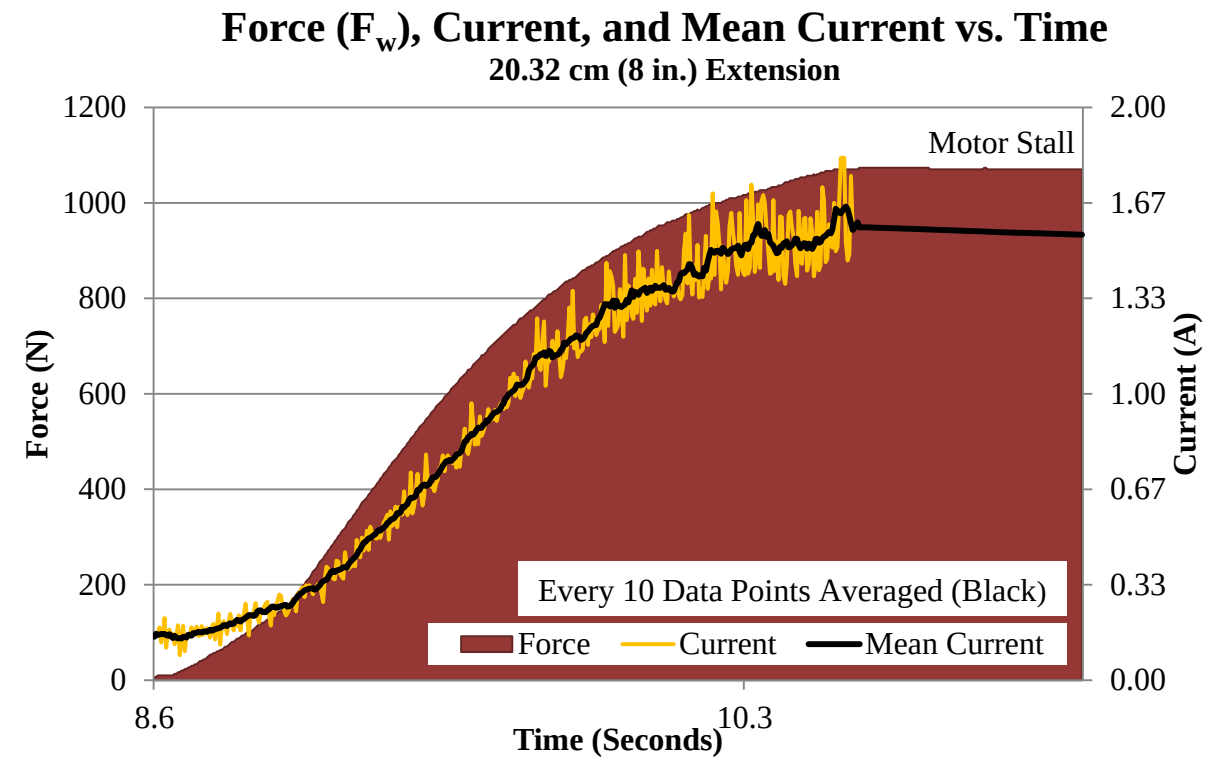

Figure 46: Force (F_w), Current, and Mean Current vs. Time at 20.32 cm (8 in.) Extension

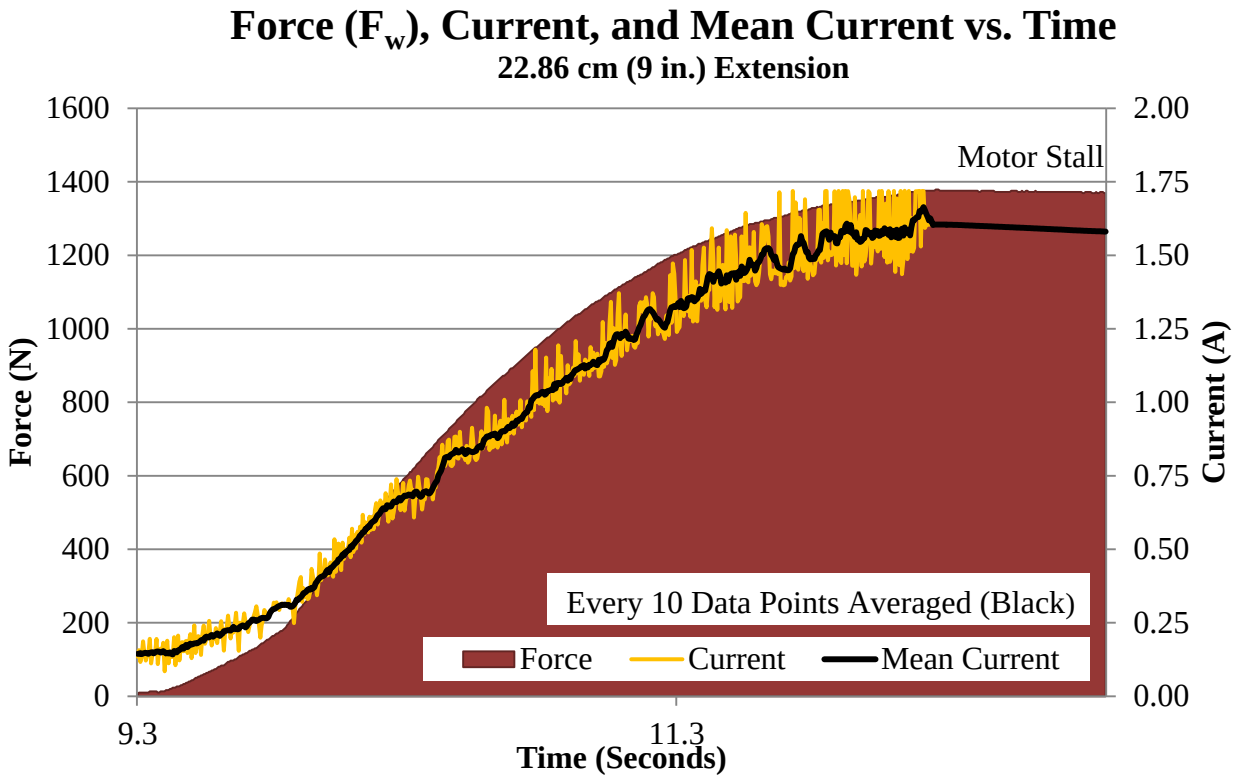

Figure 47: Force (F_w), Current, and Mean Current vs. Time at 22.86 cm (9 in.) Extension

Taking the mean of 10 current sensor values reduces the noise seen by the current sensor as needed. Third, modifying the threshold value, based on laboratory testing to take into account the error window of the FPGA, could be done. If the current sensor value gets too close to the threshold position it can prematurely stop motor operations as seen at the 18.24 cm (7.18 in.) extension in Table 9: *Current Sensor Performance*. These modifications should be verified to ensure that appropriate software changes are functioning properly at all extensions.

10.1.2 Mechanical System Sensitivity Analysis

The analyses and data displayed above in Section 8.2 *Intermediate Design Calculations Based on Initial Tests* demonstrate that the geometry and configuration of the motor to the coupling arm extension defines the forces to create the desired contact with the bore-hole wall. This section evaluates sensitivity to two parameters fundamental to these geometric relations: 1) length of the motor drive rod and 2) the location where this strut connects to the coupling arm at point Q as shown in Figure 48.

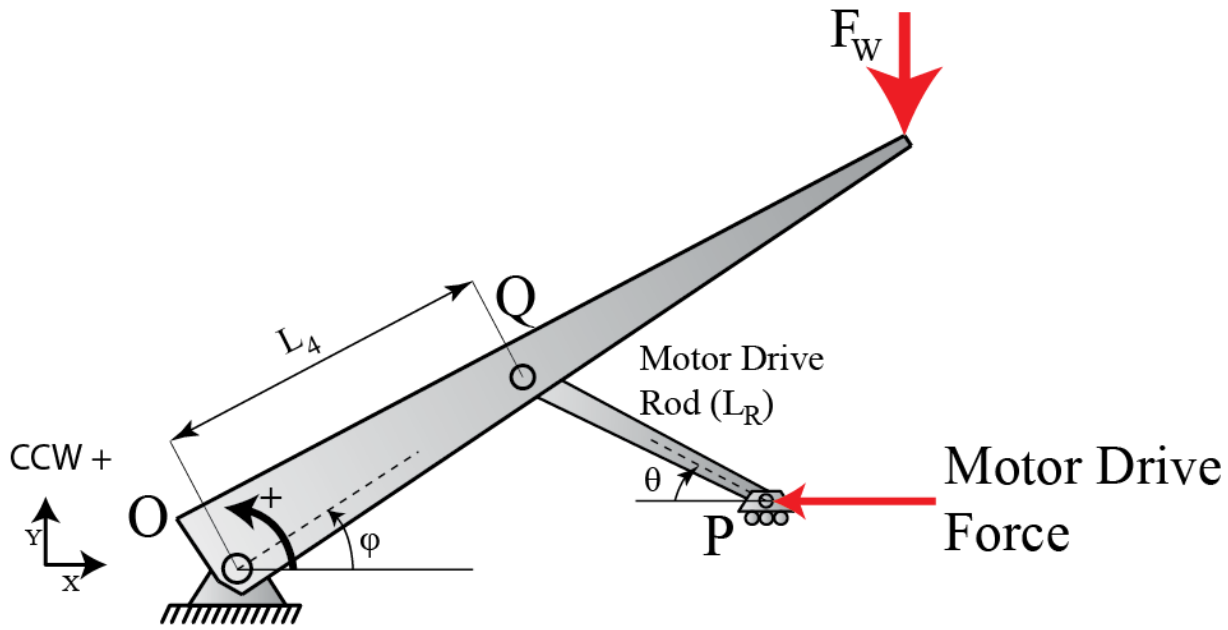

Figure 48: Configuration of Coupling Arm and Motor Drive Rod

Table 10 shows that as the length of the motor drive rod is increased, the bore-hole wall contact force decreases because the angle θ is low and less force is directed in the radial direction. And if the rod length was decreased, the opposite effect was seen.

Table 10: Predicted Motor Drive Force as Motor Drive Rod Length Changes

12.70 cm (5 in.) Extension						
Motor Drive Rod Length		θ	Motor Drive Force		Fw	
cm	in.	degrees	N	lbf.	N	lbf.
7.62	3.00	10.19	18598.16	4186.06	1777.15	400.00
10.16	4.00	7.62	19339.86	4353.00	1777.15	400.00
12.70	5.00	6.09	19471.85	4382.71	1777.15	400.00
15.24	6.00	5.07	19357.32	4356.93	1777.15	400.00
17.78	7.00	4.35	19148.68	4309.97	1777.15	400.00
17.78 cm (7 in.) Extension						
Motor Drive Rod Length		θ	Motor Drive Force		Fw	
cm	in.	degrees	N	lbf.	N	lbf.
7.62	3.00	30.74	9747.19	2193.89	1777.15	400.00
10.16	4.00	22.54	10543.18	2373.05	1777.15	400.00
12.70	5.00	17.86	11469.56	2581.56	1777.15	400.00
15.24	6.00	14.81	12173.80	2740.07	1777.15	400.00
17.78	7.00	12.65	12642.48	2845.56	1777.15	400.00
22.86 cm (9 in.) Extension						
Motor Drive Rod Length		θ	Motor Drive Force		Fw	
cm	in.	degrees	N	lbf.	N	lbf.
7.62	3.00	67.95	5922.94	1333.13	1777.15	400.00
10.16	4.00	44.04	8095.28	1822.08	1777.15	400.00
12.70	5.00	33.79	7698.89	1732.86	1777.15	400.00
15.24	6.00	27.61	7667.03	1725.69	1777.15	400.00
17.78	7.00	23.41	7866.96	1770.69	1777.15	400.00

Table 11 shows that as the application point of the motor drive rod was moved radially toward the point of contact with the bore-hole wall, the contact force increased. When the angle between the coupling arm and the motor drive rod was at 90^{o}, the maximum force was achieved. Conversely, when the angle between the coupling arm and the motor drive rod was low (when θ was near zero), contact force decreased because most of the net motor force was directed axially.

The practical result of this is that the same bore-hole wall contact force can be achieved with a lower motor force as shown in Table 11.

Table 11: Predicted Motor Drive Force as L4 Changes

12.70 cm (5 in.) Extension						
L4		θ	Motor Drive Force		Fw	
cm	in.	degrees	N	lbf.	N	lbf.
7.62	3.00	N/A	N/A	N/A	1777.15	400.00
10.16	4.00	N/A	N/A	N/A	1777.15	400.00
12.70	5.00	4.85	22702.14	5109.78	1777.15	400.00
15.24	6.00	10.02	18286.81	4115.98	1777.15	400.00
17.78	7.00	15.28	13745.29	3093.78	1777.15	400.00
17.78 cm (7 in.) Extension						
L4		θ	Motor Drive Force		Fw	
cm	in.	degrees	N	lbf.	N	lbf.
7.62	3.00	3.61	23612.57	5314.70	1777.15	400.00
10.16	4.00	11.82	18818.26	4235.60	1777.15	400.00
12.70	5.00	20.29	12878.40	2898.66	1777.15	400.00
15.24	6.00	29.26	9618.39	2164.90	1777.15	400.00
17.78	7.00	39.11	8170.72	1839.06	1777.15	400.00
22.86 cm (9 in.) Extension						
L4		θ	Motor Drive Force		Fw	
cm	in.	degrees	N	lbf.	N	lbf.
7.62	3.00	14.99	17085.85	3845.67	1777.15	400.00
10.16	4.00	27.22	11264.97	2535.51	1777.15	400.00
12.70	5.00	42.31	9454.40	2127.99	1777.15	400.00
15.24	6.00	61.70	6934.80	1560.88	1777.15	400.00
17.78	7.00	N/A	N/A	N/A	1777.15	400.00

Note: N/A indicates a non-physical condition for the geometric constraints.

Understanding these relations can be applied to engineer the point of application for the motor drive rod and the motor drive rod length to maximize bore-hole contact force for a given motor force. Lower stresses on the motor will result in longer motor life and more margin toward achieving needed coupling forces.

10.2 Conclusion

An application to control the coupling force applied to a seismic monitoring tool anchoring system was created to be deployed down-hole in high-temperature geothermal environments. This was implemented through a microprocessor and software code that monitored applied force through a current sensor on a coupling arm drive motor. Once the code was uploaded to the microprocessor with selected threshold values for the various bore-hole diameters, the system was put into a closed loop configuration and tested. When powered, the motor was signaled to turn on and the current sensor values were read verifying a voltage was less than the threshold value until the desired force was achieved. The tests verified that the motor would stop close to the correct force loads at the three pre-designated radial extensions.

REFERENCES

AltaRock Energy. (2012, March). *The Future of Geothermal Energy*. Retrieved 4 21, 2012, from http://blog.newberrygeothermal.com/

American Oil and Gas Historical Society. (2011). Shooters – A "Fracking" History. *http://aoghs.org/technology/shooters-well-fracking-history/*. Washington, D. C.: American Oil and Gas Historical Society.

Asmundsson, R., Normann, R., Lubotzki, H., & Livesay, B. (2011, 24 1). *High Temperature Tools.* Retrieved from International Partnership for Geothermal Technology: http://internationalgeothermal.org/Working_Groups/Documents/Final%20Draft%20Feb%202012%20-%20High%20Temp%20Tools%20white%20paper.pdf

Chu, P. P. (2006). *RTL Hardware Design Using VHDL*. Hoboken, New Jersey: John Wiley & Sons, Inc.

Environmental Protection Agency. (2004, June). Evaluation of Impacts to Underground Sources of Drinking Water by Hydraulic Fracturing of Coalbed Methane Reservoirs, Final Report. Washington, D. C.: Environmental Protection Agency.

Henfling, J., Greving, J., Maldonado, F., Chavira, D., & Uhl, J. (2010). Development of a HT Seismic Monitoring Tool. *Innovative Technologies for an Efficient and Reliable Electricity Supply (CITRES)* (pp. 373 - 378). IEEE.

Jefferson W. Tester, e. a. (2006). *Future of Geothermal Energy.* Retrieved 3 19, 2012, from Idaho National Laboratory: http://geothermal.inel.gov/publications/future_of_geothermal_energy.pdf

Lawrence Berkeley National Laboratory, Earth Science Division. (2012, 4 21). *EGS: Interactive, Real-Time Map of Earthquakes at The Geysers* . Retrieved 4 21, 2012, from Induced Seismicity: http://esd.lbl.gov/research/projects/induced_seismicity/egs/geysers.html

Majer, E., Baria, R., Stark, M., Smith, B., Oates, S., Bommer, J., & Asanuma, H. (2006, 9 20). *Induced Seismicity.* Retrieved 4 19, 2012, from EGS Protocols: http://www.iea-gia.org/documents/ISWPf1MajerWebsecure20Sep06.doc

Mitcham Industires, Inc. (2012). *Mitcham Industries Products*. Retrieved 4 22, 2012, from http://www.mitchamindustries.com/Products/detail.php?pId=107&cat=Sercel MaxiWave™

S.P. Lynch, Defence Science & Technology Organisation. (2007). *Progress Towards Understanding Mechanicsm Of Hydrogen Embrittlement And Stress Corrosion Cracking.* Nashville, Tennessee: NACE International.

U.S. Department of Energy. (2008). *An Evaluation of Enhanced Geothermal Systems Technology.* Washington D.C.: U.S. Department of Energy.

U.S. Department of Energy. (2012, 3 30). *Geothermal Technologies Program: Energy Basics*. Retrieved 4 21, 2012, from http://www1.eere.energy.gov/geothermal/geothermal_basics.html

Valdez, B., Schorr, M., & Arce, A. (2006). *The Influence of Minerals on Equipment Corrosion in Geothermal Brines* . Retrieved 4 19, 2012, from International Geothermal Association: http://pangea.stanford.edu/ERE/db/IGAstandard/record_detail.php?id=5514

Williams, C. F., Reed, M. J., Robert, D. H., & Jacob, G. S. (2008, 11 18). *USGS.* Retrieved 4 16, 2012, from Assessment of Moderate- and High-Temperature Geothermal Resources of the United States: http://pubs.usgs.gov/fs/2008/3082/

Zhen, Y. (2012, 8 31). *Current Sensing Circuit Concepts and Fundamentals.* Retrieved 02 24, 2012, from Microchip: http://www.microchip.com/stellent/idcplg?IdcService=SS_GET_PAGE&nodeId=1824&appnote=en551198

Appendix A. DIGITAL CONTROL OPTIONS

Digital Control Options for Motor Controller			
Comparisons (listed below)	ARM 7	8051	FPGA
Operating Temp. (°C)	200	225	240
Duration (hrs)	1000	43800	3000
Computation Speed	7	3	10
Cost Approx. ($)	6000	4000	2800

Note: Costs were driven by additional components needed to operate controller. (ADC, EEPROM, Memory, Power Source, etc.)

Constraints	ARM 7	8051	FPGA
BUILD SIZE	Yes	Yes	Yes
AVAILIBILITY	Yes	Yes	Yes

	Weight (%)	Score	Weighted Score	Score	Weighted Score	Score	Weighted Score
Operating Temp. (°C)	50	0.00	0.00	0.63	0.31	1.00	0.50
Duration (hrs)	10	0.00	0.00	1.00	0.10	0.05	0.00
Computation Speed	20	0.57	0.11	0.00	0.00	1.00	0.20
Cost ($)	20	0.00	0.00	0.63	0.13	1.00	0.20
TOTAL	100		0.11		0.54		0.90

Operating Temperature – The max operational temperature in **degrees Celsius**.

Duration – The number of **hours** the controller could operate at temperature.

Computation Speed – An estimation on a **1-10** scale (1 being very slow to 10 very fast).

Cost Approximation – The estimated cost at time.

Each item was normalized and weighed resulting in a value between 0 and 1. The higher the end value, the better the choice.

Appendix B. DC MOTOR COMPONENT TEST PROCEDURE

Purpose:

To determine if the DC motor can perform at the desired temperature.

Equipment:

1) Safety Glasses
2) 24V DC power supply (Sorensen XHR 60-18) with wires
3) 5V DC power supply (Agilent E3612A)
4) Voltage Meter (BK Precision 2707B)
5) Current Meter (TENMA 72-7732)
6) Digital Thermometer (OMEGA 2168A with K-type thermocouple)
7) Oven (Fisher Scientific Isotemp Oven Model: 851F)
8) HT DC Motor (Globe Motors: DC Permanent Magnet Gearmotor, A-2030 housing)
9) Motor Couplings
10) Unistrut Housing and Support Structures
11) Pulley with nylon string

Procedure:

Simulated Torque at Temperature:

1) Mount motor securely in oven.
2) Attach motor shaft to ¼ in drive shaft using ½ in coupling with spacers.
3) Attach pulley to ¼ in drive shaft.
4) Secure ¼ in shaft to frame with bearing to reduce chances of bending the drive shaft.
5) Attach 2 lb weight to pulley/string in a manner that it coils evenly.
6) Place thermocouple within oven ensuring cable doesn't obstruct the drive shaft.
7) Attach a red positive wire connector to DC motor (not plugged into DC power supply).
8) Attach a black negative wire from DC motor to one side of shunt resistor.
9) Attach BK Precision voltmeter to shunt amplified circuit verifying a 5V power supply is connected to circuit.
10) Attach a negative wire from remaining end of shunt resistor to current meter input.
11) Attach COM from current meter to DC power supply (NEGATIVE).
12) Turn on all power supplies.

13) Turn oven on.
14) Set desired temperature.
15) Connect the red positive wire from motor to power supply and record both current and Vout once the motor has done 1 revolution (ensuring a steady value).
16) Unplug wire from power supply and reverse polarity (swap red and black wires on motor).
17) Reconnect power supply to return weight to start position.
18) Unplug wire from power supply and reverse polarity.
19) Repeat steps 14 to 18 until motor reaches desired operational temperature of 210°C.

Pass/Fail Criteria: Motor must be operational at 210°C.

Appendix C. CURRENT SENSOR DESIGN AND TEST PROCEDURE

Purpose:

To determine the correct resistor values required to amplify the voltage division value based on a 5 volt power supply. Max Vout will equal 4V.

Equipment:

1) Safety Glasses
2) Honeywell High Temp Op-amp HTOP01
3) Supporting Resistors
4) 0.1 Ω Resistor (Shunt Resistor)
5) High Temperature Solder
6) High Temperature Soldering Iron
7) Teflon Coated Wires
8) 5V DC Power Supply (Agilent 35612A)
9) Digital Thermometer (OMEGA 2168A with K-type thermocouple)
10) Oven (Fisher Scientific Isotemp Oven Model: 851F)
11) KEITHLY 2400

Procedure:

1) Find maximum current of motor.
2) Using the following equation to determine gain required:
    a. Vout = Gain * (Shunt Resistor Value) * (Max Current)
3) Choose appropriate Resistors.
4) Construct Current Sensor.
5) Suspend Current Sensor in oven.
6) Turn on all power supplies.
7) Turn oven on.
8) Set desired temperature.
9) Connect all required wires.
10) Use KEITHLY to supply required current value when temperature is reached.
11) Repeat steps 8 to 10 until all data is collected.

Appendix D. CURRENT SENSOR

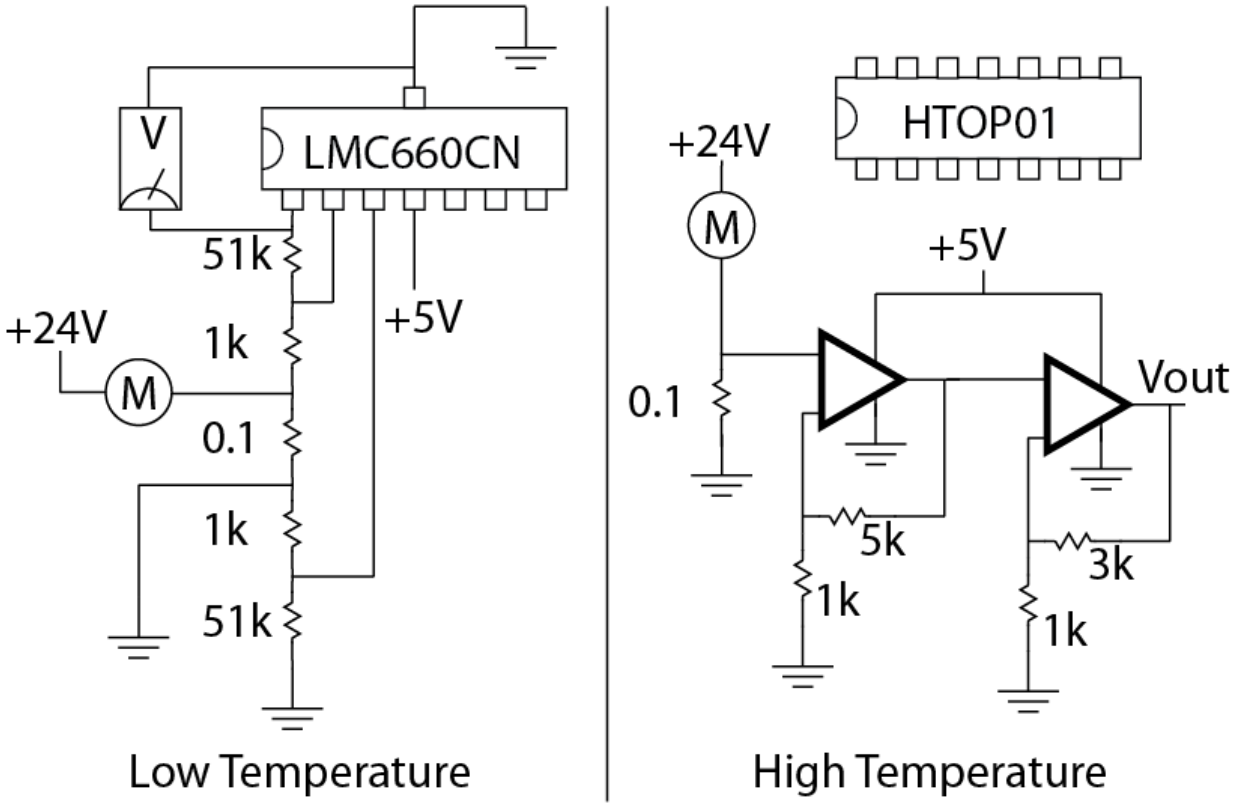

Vout = Gain*(Shunt)*(Max Current Motor)
Vout = Opamp supply voltage = 4V
4V = Gain*(0.1)*(1.78)
Gain = 22
Resistor Selection: 5k,1k and 3k,1k
Gain = (5+1)*(3+1) = 24 <- close enough
Current = Vout/(0.1*24)

Appendix E. ELECTRO-MECHANICAL SYSTEM TEST

Purpose:

To determine force produced at the end of the coupling arm.

Equipment:

1) Safety Glasses
2) 24V DC power supply (BK Precision 1761) with wires
3) Digital Thermometer (OMEGA 2168A with K-type thermocouple)
4) HT DC Motor (Globe Motors: DC Permanent Magnet Gearmotor, A-2030 housing)
5) One-Piece Rigid Coupling
6) Rigid ™ Support Frame
7) Seismic tool body
8) MTS Load Cell
9) Data Acquisition System
10) HTOP01
11) Resistors

Procedure:

Simulated Force at Various Bore-Hole Diameters:

1) Place seismic tool under MTS load cell at the point where the coupling arm will make contact with the center of the sensor.
2) Attach a red positive wire connector to DC motor (not plugged into DC power supply).
3) Attach a black negative wire from DC motor to one side of the current sensor.
4) Attach BK Precision voltmeter to current sensor's amplified circuit verifying a 5V power supply is connected to circuit.
5) Attach the Vout wire from the current meter to the positive terminal on the DAS.
6) Attach the ground of the DAS to the same ground current sensor is attached to.
7) Connect the thermocouple to the DAS
8) Configure DAS to record data to specified location.
9) Turn on power supplies.
10) Turn hydraulic system on.
11) Set desired coupling arm extension height (on the load cell).
12) Run DAS capture software.

13) Connect the red positive wire from motor to power supply and record data from test (force, temperature, and Vout) until the motor reaches 1779 N (400 lbf.) or stalls.
14) Unplug wire from power supply then reconnect a few times to ensure force is stable.
15) Remove positive wire from power supply.
16) Stop DAS.
17) Remove current sensor from circuit (unplug wire from motor ground).
18) Reverse polarity (swap red and black wires on motor).
19) Reconnect power supply to remove force on load cell.
20) Adjust load cell for next coupling arm extension (ensuring to lock the load cell in place).
21) Unplug wires from power supply, reverse polarity, and connect current sensor.
22) Modify DAS save location for next trial run.
23) Repeat steps 11 to 22 until all coupling arm extension force values are obtained.
24) Remove tool and turn off hydraulic system.

Pass/Fail Criteria: Motor must be capable of producing 1779 N (400 lbf.) at all coupling arm extensions.

Appendix F. COUPLING ARM CALCULATIONS

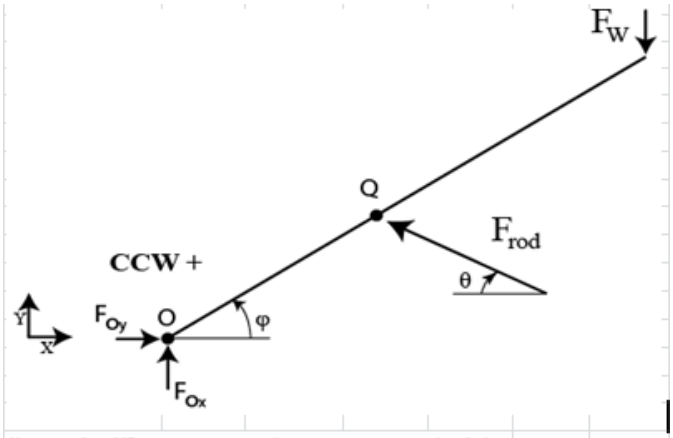

(Increasing V3 measurement because easy to obtain)

**Note: V3 is measured from arm tip to rotation point O (Add 1.18 to get distance to bottom of tool)*

TOOL EXTENSION	4.18	5.18	6.18	7.18	8.18	9.18
V3	3.00	4.00	5.00	6.00	7.00	8.00
Sin(phi)	0.21	0.28	0.35	0.42	0.49	0.56
phi (deg)	12.09	16.22	20.44	24.77	29.26	33.96
Cos(phi)	0.98	0.96	0.94	0.91	0.87	0.83
Tan(phi)	0.21	0.29	0.37	0.46	0.56	0.67
L1	5.75	5.65	5.51	5.34	5.13	4.88
V2	0.08	0.53	1.01	1.53	2.11	2.78
Sin(theta)	0.02	0.16	0.31	0.47	0.65	0.86
theta(deg)	1.41	9.40	18.12	28.15	40.59	58.82
Cos(theta)	1.00	0.99	0.95	0.88	0.76	0.52
L2	3.25	3.21	3.09	2.87	2.47	1.68
L3	5.00	4.90	4.82	4.80	4.90	5.32
Frod Required	3998.95	2107.87	1413.90	1058.98	855.70	763.44
Fw Predicted	400.00	758.86	1131.32	1510.49	1869.33	2095.22
FW Predicted (F)	100.69	123.45	165.66	217.88	284.61	280.05
Frod Max	1006.62	650.54	585.55	576.82	608.84	534.51
Fw Measured:	101.01	116.86	177.98	237.60	241.38	310.05
Error:	0.31	5.64	6.93	8.30	17.91	9.68

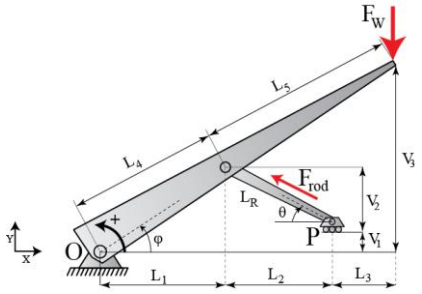

Procedure for Estimating Frictional Forces:

1 Calculate the net F_x forces of F_{rod} without friction at all positions.
2 Estimate motor net force with no friction where θ is near zero (4.14" extension).
3 Estimate frictional forces lost by subtacting the net F_x from the value in Step 2.
4 Calculate F_y from measured F_w.
5 Divide frictional force by F_y to calculate a frictional coefficient.
6 Plot frictional coefficient as a function of sine θ and create a trendline.
7 Using trendline formula, calculate frictional coefficient at θ = 0.
8 Calculate frictional forces near zero and add this to the net motor force estimated in Step 2. Set this equal to maximum motor force.
9 Repeat these steps starting at Step 1 including the frictional forces calculated in the first iteration. Make adjustments as appropriate.

With these formulas of friction coefficient and maximum motor force, net forces on F_{rod} can be predicted.

Constants	
V1	1.18
L4	5.88
L5	8.44
LR	3.25
Half Tool Weight	0

L4+L5:	14.32
5.88	
	5.88
3.25	

From test we know we got 300 lbf @ V3=8

Step	Equation
1	V3/(L4+L5)=Sin(phi)
2	L1/L4 = Cos(phi)
3	(V2+V1)/L4 = Tan(phi)
4	V2/LR = Sin(theta)
5	L2/LR = Cos(theta)
6	(L1+L2+L3)/(L4+L5) = Cos(phi)

Fw	400.00	<-Based on Test Value
Frod Required	3998.95	<-Based on Fw value

Obtained from physical test; Max Value from Load Cell Data
Change Frod to Fw measured location where V3 = 8

Moment Equation about point O

*Mo = -Fw(L1 + L2 + L3) + Frod(L1*Sin(theta) + (V1 + V2)*Cos(theta))+V3*(Half Tool Weight)*

*Frod = (Fw(L1 + L2 + L3)-V3*Half Tool Weight)/(L1*Sin(theta) + (V1 + V2)*Cos(theta))*

Reaction Forces At O		*Force on pin, point P*
Rx = ΣFx=0	Ry=Σfy = 0	*Fx = Frod*Cos(theta)*
FOx + L4*cos(ϕ)*Frod = 0	FOy - Fw + L4*sin(ϕ)*Frod = 0	*Fy = Frod*Sin(theta)*

Appendix G. GEARBOX CALCULATIONS

Required Motor Torque			
RATIO	**MAX TORQUE (oz-in.)**	**MAX TORQUE (Nm)**	**MAX Fw (N)**
524.60	366.00	2.58	448.73
639.90	445.00	3.14	545.59
780.60	544.00	3.84	666.97
2077.62	**1449.50**	**10.24**	**1777.15**

Using the knowledge that 1779 N (400 lbf.) is the required force at the bore-hole wall at the 10.62 cm (4 in.) extension, allows the gearing ratio required to be solved for.

Step 1: Solve for Max Torque

$$\frac{Max\ Torque\ (Unknown)}{1777.15\ N} = \frac{2.58\ Nm}{448.73\ N}$$

Step 2: Solve for Ratio

$$\frac{Ratio\ (Unknown)}{10.24\ Nm} = \frac{524.60}{2.58\ Nm}$$

Appendix H. DC MOTOR DATA SHEET

Theoretical stall is 1.79 amps. When power is first applied to the motor, you will see a momentary current spike and then it drops severely to its running current. The momentary spike can be as high as the theoretical stall current. For the 5A4445 no load and rated load performance should fall within the parameters below:

Test Voltage	**(V)**	**24**
No Load Speed	(rpm)	14.1 ~ 17.0
No Load Current	(A)	0.20 Max
Normal Rated Load	(oz-in)	344
Normal Rated Load Speed (reference rpm)	10.0 ~ 12.3	
Normal Rated Load Current	(A)	.70 Max

Appendix I. INTEGRATED SOFTWARE-ELECTRO-MECHANICAL SYSTEM TEST

Purpose:

To verify the current sensor will stop the coupling arm extension when the required force is reached.

Equipment:

1) Safety Glasses
2) 24V DC power supply (BK Precision 1761) with wires
3) Digital Thermometer (OMEGA 2168A with K-type thermocouple)
4) HT DC Motor (Globe Motors: DC Permanent Magnet Gearmotor, A-2030 housing)
5) One-Piece Rigid Coupling
6) Rigid ™ Support Frame
7) Seismic tool body
8) MTS Load Cell
9) Data Acquisition System
10) HTOP01
11) Resistors

Procedure:

Simulated Force at 3 Bore-Hole Diameters (7,8,and 9):

1) Place seismic tool under MTS load cell at the point where the coupling arm will make contact with the center of the sensor.
2) Attach a red positive wire connector to DC motor (not plugged into DC power supply).
3) Attach a black negative wire from DC motor to one side of the current sensor.
4) Attach BK Precision voltmeter to current sensor's amplified circuit verifying a 5V power supply is connected to circuit.
5) Attach the Vout wire from the current meter to the positive terminal on the DAS.
6) Attach the ground of the DAS to the same ground current sensor is attached to.
7) Connect the thermocouple to the DAS
8) Configure DAS to record data to specified location.
9) Turn on power supplies.
10) Turn hydraulic system on.

11) Set desired coupling arm extension height (on the load cell).
12) Run DAS capture software.
13) Connect the red positive wire from motor to power supply and record data from test (force, temperature, and Vout) until the motor reaches 1779 N (400 lbf.) or stalls.
14) Unplug wire from power supply then reconnect a few times to ensure force is stable.
15) Remove positive wire from power supply.
16) Stop DAS.
17) Remove current sensor from circuit (unplug wire from motor ground).
18) Reverse polarity (swap red and black wires on motor).
19) Reconnect power supply to remove force on load cell.
20) Adjust load cell for next coupling arm extension (ensuring to lock the load cell in place).
21) Unplug wires from power supply, reverse polarity, and connect current sensor.
22) Modify DAS save location for next trial run.
23) Repeat steps 11 to 22 until all coupling arm extension force values are obtained.
24) Remove tool and turn off hydraulic system.

Pass/Fail Criteria: Extension forces should be limited based on threshold value.